Muscle architecture and muscle fibre type composition in the forelimb of two African mole-rat species, *Bathyergus suillus* and *Heterocephalus glaber*

L. Sahd[1, 2], N. Doubell[1], N.C. Bennett[3], S. H. Kotzé[1, 4]

[1] Division of Clinical Anatomy, Department of Biomedical Sciences, Faculty of Medicine and Health Sciences, Stellenbosch University, Cape Town 8000, South Africa

[2] Evolutionary Developmental Biology Research Group, Department of Biology, Ghent University, Ghent 9000, Belgium.

[3] Mammal Research Institute, Department of Zoology and Entomology, University of Pretoria, Pretoria 0002, South Africa

[4] Division of Anatomy, Department of Biomedical Sciences, Ross University School of Veterinary Medicine,

Basseterre, St Kitts and Nevis, West Indies

Running Title: Functional forelimb morphology of mole-rats

Editorial correspondence:

Prof S.H. Kotzé

Postal address: Department of Biomedical Sciences, Faculty of Medicine and Health Sciences, Stellenbosch University, PO Box 241, Cape Town, 8000, South Africa

Email: shk@sun.ac.za

DATA AVAILABILITY STATEMENT

The data that support the findings of this study are available from the corresponding author upon reasonable request.

FUNDING INFORMATION

National Research Foundation of South Africa (NRF); Grant number: 120827

CONFLICT OF INTEREST

The authors have no conflict of interest to declare.

ETHICAL APPROVAL STATEMENT

Ethical clearance was obtained for the use of animal tissue from the Research Ethics Committee: Animal Care and Use of Stellenbosch University (SU-ACUM 16-00005). Ethical clearance was extended for the present study under a new number, ACU-2020-19344. Additionally, ethical clearance was obtained from the Ethics committee of the University of Pretoria (EC069-17).

AUTHOR ORCID ID:

Lauren Sahd: https://orcid.org/0000-0002-6854-6996

Narusa Doubell: https://orcid.org/0000-0002-6684-4551

Nigel Bennett: https://orcid.org/0000-0001-9748-2947

Sanet Kotzé: https://orcid.org/0000-0003-0853-2178

ABSTRACT

The scratch-digging Cape dune mole-rat, (*Bathyergus suillus*) and chisel toothed digging naked mole-rat, (*Heterocephalus glaber*) are African mole-rats that differ in their digging strategy. The aim of this study was to determine if these behavioural differences are reflected in the muscle architecture and fibre type composition of the forelimb muscles. Muscle architecture parameters of 39 forelimb muscles in both species (n=6 each) were compared. Furthermore, muscle fibre type composition of 21 forelimb muscles were analysed using multiple staining protocols. In *B. suillus*, muscles involved with the power stroke of digging (limb retractors and scapula elevators), showed higher muscle mass percentage, force output and shortening capacity compared to those in *H. glaber*. Additionally, significantly higher percentages of glycolytic fibres were observed in the scapular elevators and digital flexors of *B. suillus* compared to *H. glaber,* suggesting that the forelimb muscles involved in digging in *B. suillus* provide fast, powerful motions for effective burrowing. In contrast, the *m. sternohyoideus* a head and neck flexor, had significantly more oxidative fibres in *H. glaber* compared to *B. suillus.* In addition, significantly greater physiological cross-sectional area (PCSA) and fascicle length values were seen in the neck flexor, *m. sternocleidomastoideus,* in *H. glaber* compared to *B. suillus*, which indicates a possible adaptation for chisel-tooth digging. While functional demands may play a significant role in muscle morphology, the phylogenetic differences between the two species may play an additional role which needs further study.

Keywords: thoracic limb, PCSA, burrowing, Bathyergidae, histology

RESEARCH HIGHLIGHTS:

Large architectural values and large numbers of glycolytic fibres were seen in essential scratch-digging muscles of *B. suillus*. However, the neck muscles of *H. glaber* had a fast shortening capacity or excursion, indicating possible adaptations for chisel-tooth digging.

1. INTRODUCTION:

Multiple studies on subterranean rodents have suggested that species-specific behaviours such as hind foot-drumming, chisel-tooth digging and scratch-digging may influence the morphology of their limbs (Lehmann, 1963; Hildebrand, 1985; Fransescoli, 2000; Rose, Sandefur, Huskey, Demler & Butcher, 2013; Sahd, Bennett & Kotzé, 2019; 2020; 2021; 2022a; Sahd, Doubell, Bennett & Kotzé, 2022b). Subterranean rodents exhibit different methods of soil excavation during burrowing, which may be influenced by their unique habitat, such as soil hardness, rainfall and type of vegetation cover (Hildebrand, 1985; Lessa, Vassallo, Verzi & Mora, 2008; Kubiak et al., 2018), or phylogeny (Lehmann, 1963).

Bathyergus suillus (the Cape dune mole-rat; Schreber, 1782) is a solitary species and the largest member of the family Bathyergidae and can weigh up to 2kg in body mass (Bennett & Faulkes, 2000). This species prefers mesic regions with sandy soils in the coastal regions of the Cape Peninsula and sands of the western and southern Cape in South Africa (Skinner & Smithers, 1990; Bennett & Faulkes, 2000). They are known as scratch-diggers and use their well-developed foreclaws and short forelimbs to dig their burrow systems and to loosen the sandy soils which they inhabit (Bennett & Faulkes,

2000). Furthermore, *B. suillus* uses hind foot-drumming to produce seismic signals for communication (Bennett & Jarvis, 1988; Hart, O'Riain, Jarvis, Bennett, 2006).

Heterocephalus glaber (the naked mole-rat, Rüppell, 1842) is the smallest member of the family Bathyergidae with a mean body mass of 34g (Bennett & Faulkes, 2000). In this eusocial species, colony members are in constant close proximity (Jarvis & Sale, 1971; Bennett & Faulkes, 2000) and use vocalisations and tactile signalling to communicate (Bennett & Jarvis, 1988; Pepper, Braude, Lacey, Sherman, 1991). *Heterocephalus glaber* is endemic to dry regions of eastern Africa (Brett, 1991; Honeycutt, Allard, Edwards & Schlitter, 1991). It is a known as a chisel-tooth digging species as it uses its procumbent incisors to dig burrows in hard, compact, lateritic soils (Brett, 1991, Bennett & Faulkes, 2000). The non-reproductive workers of the colony work co-operatively to excavate extensive burrow systems that can be several hundred meters in length. (Brett 1991; Bennett & Faulkes, 2000; Kutsukake, Inada, Sakamoto & Okanoya, 2019).

Muscle architectural properties such as fibre length, muscle mass and PCSA have been documented in the forelimb muscles of scratch-digging terrestrial animals such as the badger (*Taxidea taxus*; Moore, Budny, Russell & Butcher, 2013), nine banded armadillo (*Dasyspus novemcinctus*; Olson, Woble, Thomas, Glenn & Butcher, 2016), groundhog (*Marmota monax;* Rupert, Rose, Organ & Butcher, 2015) as well as the subterranean Eastern mole (*Scalopus aquaticus;* Rose, et al., 2013). Muscle architecture is a determinant and reflection of muscle function. Moreover, muscle architectural properties determine the force with which the muscle contracts and plays an important role in understanding the structure-function relationship of muscles (Sacks & Roy,

1982; Lieber & Fridén, 2000; Eng, Smallwood, Rainiero, Lahey, Ward &Lieber 2008; Rupert et al., 2015). Muscle fibre length is an important aspect of muscle architecture (Lieber & Ward, 2011) as it is directly proportional to the muscle excursion (the displacement of the myotendinous junction throughout the range of motion). A long muscle fibre has many serial sarcomeres that act as a single muscle fascicle when activated. This leads to higher maximum muscle velocity and ultimately permits a greater muscle excursion (Bodine et al., 1982; Winters, Takahashi, Lieber & Ward, 2010; Lieber & Ward, 2011) compared to muscles with short fibre lengths. Furthermore, the isometric force of a muscle is proportional to the physiological cross-sectional area (PCSA). The PCSA is calculated using various parameters, including fascicle length, pennation angle and muscle volume (Gans & Bock, 1965; Gans & De Vries, 1987). The isometric force-velocity relationship suggests that muscles with high shortening velocity led to low force production, whereas muscles with low shortening velocities produce large forces. Therefore, large PCSA and long fascicle length are both indicators of a powerful muscle (Lieber & Ward, 2010; Moore, et al., 2013). However, there are multiple components that determine the functional properties of a muscle in addition to the architectural properties (Talbot & Maves, 2016). Therefore, combining muscle architecture and other properties such as muscle fibre type composition, contribute to the understanding of muscle function (Eng et al., 2008).

There are four main myosin heavy chain (MHC) isoforms that can be expressed in adult muscle fibres, and these include I, IIA, IIB and IIX (Eng et al., 2008; Talbot & Maves, 2016; Serrano, Perez, Lucia, Chicharro, Quiroz-Rothe & Rivero, 2001; Acevedo and Rivero, 2006; Hyatt, Roy, Rugg & Talmadge, 2006). The MHC isoform of an individual muscle fibre affects the contractile properties of the muscle fibre, namely

myosin ATPase activity, contraction velocity of the fibre, the filament sliding velocity and the power output of the fibre (Bottinelli, Canepari, Reggiani & Stienen, 1994; Schiaffino & Reggiani, 2011). All four muscle fibre types can be expressed in a single muscle. MHC I fibres are slow-contracting fibres, resistant to fatigue, and have a high mitochondrial density. MHC IIaA, IIB and IIX are fast-twitch fibres, but type IIB fibres have lower fatigue resistance compared to MHC IIX (Peter, Barnard, Edgerton, Gillespie & Stempel, 1972; Talbot & Maves, 2016). Additionally, hybrid MHC expression resulting in subtypes of muscle fibres such as MHC I/IIA or IIA/IIX (Rivero, 2018) is possible. Thomas, Chadwell, Walker, Budde, VandeBerg & Butcher (2017) suggested that MHC expression is constrained by phylogeny, but that subtle changes can occur due largely to behavioural differences between terrestrial and arboreal animals. Metabolic transformation of oxidative and glycolytic fibres may occur more dramatically due to functional demands (Yan, Okutsu, Akhtar & Lira, 2011). Kohn, Burroughs, Hartman & Noakes, (2011a); Kohn, Curry & Noakes (2011b); Curry, Hohl, Noakes & Kohn, (2012) further suggest a lack of correlation between MHC isoform and muscle energy metabolism. Therefore, muscle fibres may have different metabolic properties than the MHC gene expression would suggest. For example, an MHC I muscle fibre may have a glycolytic and/or oxidative metabolism (Kohn, Hoffman & Myburgh, 2007).

Therefore, by comparing two species that differ in both digging and communication strategies, and combining muscle architecture and muscle fibre type composition, will contribute to a more complete understanding of their muscle function (Eng et al., 2008). The aim of the present study was to determine if the muscle architecture and fibre type composition of the muscles in the forelimb and neck of *B. suillus* and *H. glaber* are

influenced by their digging mode and possible stabilization function during hind foot-drumming. The present study hypothesises that the neck muscles of *H. glaber* will indicate architectural adaptations for chisel tooth digging such as large PCSA values, and that these muscles will have more type II fibres compared to that in the forelimb of the scratch-digging *B. suillus*. Additionally, the present study hypothesises that the limb retractors and digital flexors of *B. suillus* will be powerful muscle groups (i.e., with large PCSA values and long fascicles). Furthermore, it is hypothesised that these two muscle groups will have more type II muscle fibres to account for the quick contractions needed for scratch digging in *B. suillus*.

2. MATERIALS AND METHODS

2.1. Sample

Ethical clearance was obtained for the use of animal tissue from the Research Ethics Committee: Animal Care and Use of Stellenbosch University (SU-ACUM 16-00005). Ethical clearance was extended for the present study under a new number, ACU-2020-19344 and the Ethics committee of the University of Pretoria (EC069-17). The *B. suillus* (Stellenbosch University: 10NP_VAN01; University of Cape Town: 200/V7/JOR University of Pretoria EC069-17) and *H. glaber* (University of the Western Cape: ScR1RC2007/3/30) specimens were obtained from previous unrelated studies. No animals were specifically killed for the present study.

The left forelimbs of 12 formalin fixed specimens (n=6 per species) were used for muscle architecture analysis, unless multiple muscles were damaged, and the right limb was used. The right forelimbs of six frozen *B. suillus* specimens and six formalin fixed *H. glaber* specimens were used for the muscle fibre typing.

2.2. MUSCLE ARCHITECTURE

Thirty-nine muscles were dissected from origin to insertion on each limb, as previously described by Doubell, Sahd & Kotzé (2020), after which the muscles were removed. Four architectural parameters were measured for each of the 39 forelimb muscles in each specimen based on techniques described by Payne, Hutchinson, Robilliard, Smith & Wilson (2005) and Martin, Warburton, Travouillon & Fleming (2019). Muscle mass was measured to the nearest 0.001 g using a digital scale (*Ohaus Adventurer Pro AV3102, Nanikon, Switzerland*). A Mastercraft digital sliding calliper (150mm measuring range) was used to measure the muscle belly length (L_M; length between the origin of the most proximal muscle fibres and the insertion of the most distal fibres) to the nearest 0.001 mm. High magnification photographs were taken of each muscle using a Leica MZ67 Stereomicroscope (*Leica Biosystems, Wetzlar, Germany*). Composite images were then created using Image Composite Editor (Microsoft 2.0.3) after which six to eight random fascicles per muscle were chosen to measure the fascicle length (L_f) using the 'segmented line tool' in ImageJ (Java 1.8.0_112; Schneider, Rasband, & Elceiri, 2012; RRID:SCR_003070). Additionally, five random fascicles per muscle were chosen to measure the pennation angle (θ) using the 'angle tool' in ImageJ. Muscle mass and L_f values were increased with 14% and 11%, respectively, according to the correction factors used by Kikuchi & Kuraoka (2014), since formalin fixation causes shrinkage of muscle tissue. The mammalian skeletal muscle density (ρ) was determined as 0.001056 g/mm^3 according to Mendez & Keys (1960) and Ward & Lieber (2005). The physiological cross-sectional area (PCSA) of each muscle was calculated using a formula described by Sacks & Roy (1982) and Charles, Cappellari, Spence, Hutchinson & Wells (2016).

$$PCSA\ (mm^2)\ =\ [M_m(g) \times cos\theta]/\ [L_f(mm)\ \times \rho(g/mm^3)]$$

Additionally, the maximum isometric force (F_{max}) of contraction was estimated by multiplying the PCSA by a maximum isometric stress of 0.3 N/mm^{-2} (Medler, 2002). However, this is only an estimation of the maximum isometric force because of the variation in the displacement of the myotendinous junction throughout the range of motion (Fukunaga, Roy, Shellock, Hodgson & Edgerton, 1996). Last, an architectural index (AI) was determined by calculating the fascicle length to muscle length ratio (L_f/L_M), which is proportional to the shortening capacity (Sharir, Milgram & Shahar, 2006; Charles et al., 2016).

The 39 selected muscles were categorised according to their main functions into thirteen functional muscle groups for statistical analysis (Table 1; Olson et al., 2016; Martin et al., 2019). Biarticular muscles, crossing two joints and having more than one function, were placed into more than one functional muscle group, such as *mm. biceps brachii* and *triceps brachii caput longum* (Rupert et al., 2015; Olson et al., 2016; Böhmer et al., 2017) (Table 1). The biarticular muscles were only included in one muscle group when determining the muscle mass distribution (*m. biceps brachii* in the elbow flexors and *m. triceps brachii caput longum* in the elbow extensors). There are species differences in the absence and presence of specific muscles: *mm. coracobrachialis, tensor fasciae antebrachium* and *abductor digiti I longus,* were absent in *H. glaber,* while *m. deltoideus pars clavicularus* was absent in *B. suillus* (Doubell et al., 2020).

Table 1: List of muscle function groups

Muscle group	**Muscle**
Head flexors and hyoid bone depressors (HH)	*M. sternocleidomastoideus* (*m. cleidomastoideus and m. sternomastoideus measured as one muscle due to common tendon of insertion*)
	M. sternohyoideus
Scapular elevators/stabilizers/rotators (SE)	*M. trapezius pars cervicales*
	M. trapezius pars thoracica
	M. rhomboideus cervicis
	M. rhomboideus capitis
	M. serratus ventralis
	M. subclavius
	M. omotransversarius
	M. scapuloclavicularis
Limb retractors (LR)	*M. latissimus dorsi*
	M. pectoralis superficialis
	M. infraspinatus
	M. teres major
	M. deltoideus pars acromialis
	M. deltoideus pars scapularis
	M. deltoideus pars clavicularis (only in *H. glaber*)
	M. triceps brachii caput longum
Limb protractors (LP)	*M. subscapularis*
	M. supraspinatus
	M. coracobrachialis (only in *B. suillus*)
	M. biceps brachii
Elbow extensors (EEX)	*M. triceps brachii caput longum*
	M. triceps brachii caput laterale
	M. triceps brachii caput mediale
	M. tensor fasciae antebrachium (only in *B. suillus*)
Elbow flexors (EF)	*M. biceps brachii*
	M. brachialis
Carpal flexors (CF)	*M. palmaris longus*
	M. flexor carpi ulnaris

	M. flexor carpi radialis
Carpal extensors (CE)	*M. extensor carpi radialis* *M. extensor carpi ulnaris*
Digital flexors (DF)	*M. flexor digitorum superficialis* *M. flexor digitorum profundus*
Digital extensors (DEX)	*M. extensor digiti I longus* *M. extensor communis digitorum* *M. abductor digiti I longus* (only in *B. suillus*) *M. extensor digitorum lateralis*
Supinators (S) [a]	*M. supinator*
Pronators (P)[a]	*M. pronator teres*

[a] Studied as individual muscles

2.2.1. Statistical analysis

The mean (± standard deviation) of the muscle architectural parameters for each species were reported. Ordinary Least Squares (OLS) regressions of $\log_{10}$-transformed data of the M_M, L_f and PCSA for each individual muscle as well as the functional muscle groups, were plotted against $\log_{10}$ of body mass to determine the scaling coefficients for each species. The two species studied here scaled allometrically to body mass for all the parameters. Thus, $\log_{10}$ body mass was used as the covariate to compare the $\log_{10}$-transformed data. A one-way analysis of covariance (ANCOVA) was performed to determine significant differences within the muscle groups as well as the individual muscles between the two species (Sahd et al., 2021). Fischer's Least Significant Difference (LSD) *post-hoc* test was used to determine the p-values with a $p < 0.05$ indicating statistically significant results. Statistica 13.5 (*TIBCO software, Palo Alto, California, USA*; RRID:SCR_014213) was used to perform all statistical analysis. All graphs were created using ggplot2 (Wickham, 2016; RRID: SCR_014601) in R (R Core team; RRID:SCR_001905).

2.2.2. Functional space plots

The scatter plots of the mean PCSA (normalised to body mass, $PCSA/M_b^{0.67}$) of each individual muscle and muscle group were plotted against mean L_f (normalised to body mass, $L_f/M_b^{0.33}$) in both species (Martin et al., 2019). The normalization of parameters to body mass allowed comparison between species as there was a large difference in body size between the two species.

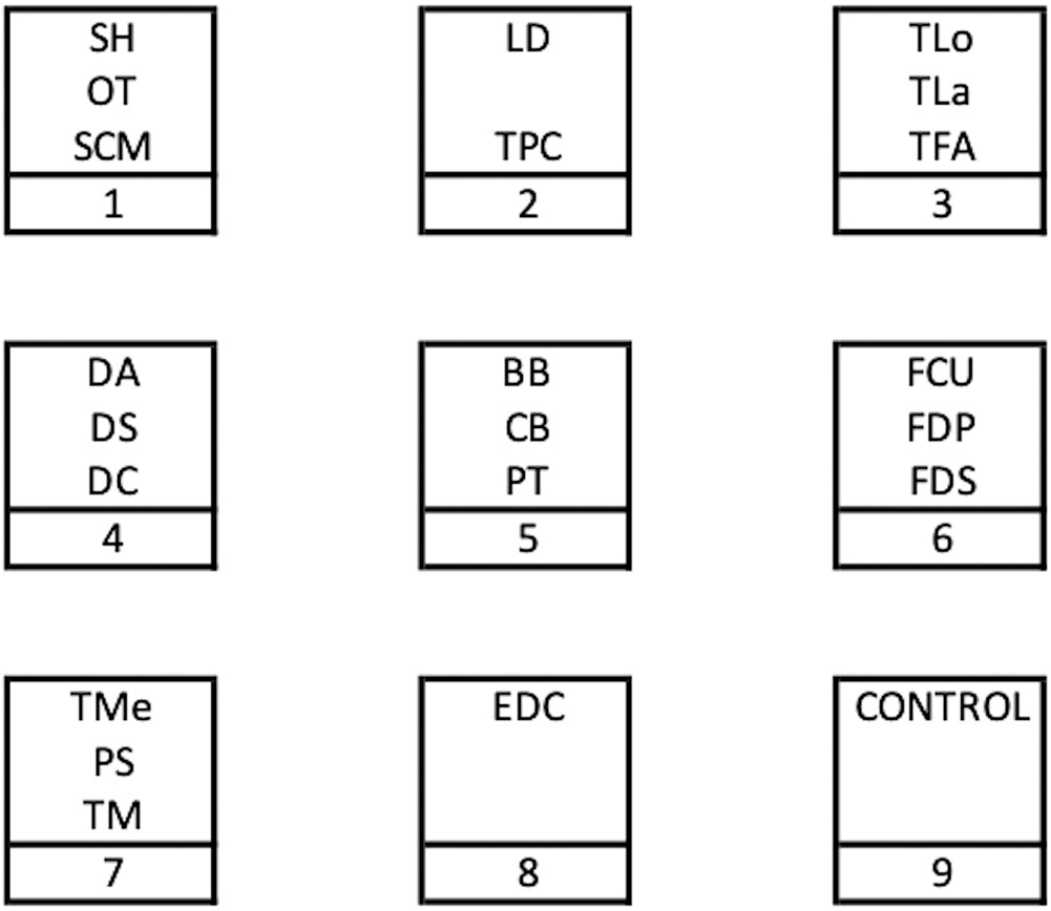

Figure 1. Slide layouts for the placement of muscle sections. See Tables 4 and 5 for muscle abbreviations.

2.3. MUSCLE FIBRE TYPING

Twenty-one specific forelimb muscles were chosen based on a similar study on the nine-banded armadillo (*Dasypus novemcinctus*; Olson et al., 2016). A layout (Figure 1) was designed of the muscle arrangement on the histology slides to ensure accurate identification of specific muscles.

2.3.1. Bathyergus suillus

Tissue preparation and sectioning

After individually thawing each specimen, small sections from the mid-bellies of each muscle were harvested from the frozen *B. suillus* specimens. The muscle sections were snap-frozen in liquid nitrogen (-170°C) and stored in a -80°C freezer overnight to allow for optimal cryostat sectioning of samples. Cross-sections of the mid-belly of each muscle were positioned onto labelled squares of cork and tissue freezing medium (OCT, *Leica Biosystems: Wetzlar, Germany*) was placed around the muscle to keep it in the correct orientation. The freezing medium and muscle tissue were sprayed with Pellox freezing spray (*Cell Path Services, Midrand, South Africa*) to keep the tissue frozen during sectioning. The muscles were sectioned at -15°C using a Leica CM1520 Cryostat (*Leica Biosystems, Wetzlar, Germany*) and one 7µm section of each muscle was placed onto positively charged slides according to the slide layout. Three slides of the exact same slide layout were produced using serial sections: one slide for each staining method and a backup slide which was stored in a dust-free container in a -20°C freezer.

Staining

Immunohistochemistry was performed with the NovoCastra Lyophilized Mouse Monoclonal Antibody Myosin Heavy Chain (slow; CAS: NCL-MHCs; LOT: 6065928; *Leica Biosystems: Wetzlar, Germany*; RRID: AB_563898) to identify slow isoform within the MHC fibres. A Novolink Polymer detection system (CAS: RE7150-CE; LOT: 6029001; *Leica Biosystems: Wetzlar, Germany*) and diaminobenzidine tetrahydrochloride (DAB; LOT: 6072346; *Leica Biosystems: Wetzlar, Germany*) were used to detect positive staining of the MHC I fibres. This staining protocol is similar to the protocol described by Kalmar, Blanco & Greensmith (2012) and Sahd et al. (2022b). Briefly, the frozen slides were brought to room-temperature prior to staining. The slides were washed in TRIS buffered saline (TBS, pH 7.6) for two increments of five minutes after which each individual tissue section was circled using a Novopen (NCL-Pen; *Leica Biosystems: Wetzlar, Germany*) reagent pen, which kept the reagents within the welled area. After applying 50µl of the primary antibody onto each tissue section (MHCs: TRIS; 1:40 dilution), the slides were placed in a plastic humidity chamber and incubated for one hour at 37°C (TC2323 SHEL LAB CO_2 Incubator, *Sheldon Manufacturing Inc.: Cornelius, Oregon, United States*). Between each step the slides were washed in TBS for two increments of five minutes each. Three to five drops of Novolink post-primary antibody (secondary antibody) were applied to each section and incubated for 15 minutes at room temperature. The same procedure was followed for the Novolink Polymer (3-5 drops; 15 minutes incubation). After the last TBS wash, 50µl of DAB solution (1:20 dilution of Novolink DAB chromogen and Novolink DAB substrate buffer) was applied to each tissue section and incubated for five minutes at room temperature. Slides were counterstained with Meyer's haematoxylin for one minute

before washing the slides in tap water. After counterstaining, the slides were washed in running tap water for five minutes and dehydrated in a series of ethanol (70%, 96%, 96%, 99%, 99%), cleared in xylene and mounted using DPX mounting media. Cross sections of the *m. biceps femoris* of a rat was used as a positive control for all runs. The primary antibody and Novolink Polymer detection system was tested on *m. biceps femoris* sections was tested for each element before being applied to the mole-rat sections.

The second staining method used *B. suillus* muscle tissue, β-nicotinamide adenine dinucleotide, reduced disodium salt hydrate (β-NADH; CAS: 606-68-8; *Sigma-Aldrich: Missouri, United States*) with nitroblue tetrazolium salt (*Sigma-Aldrich* CAS: 298-83-9) was applied to detect the levels of oxidative enzymes within the muscle fibres. Fibres with a high oxidative capacity stained dark blue and fibres with low oxidative capacity stained a light blue. Prepared slides were removed from the -20°C freezer and allowed to reach room temperature. Five to seven drops of NADH solution were applied to each tissue section after which the slides were placed in a humidity chamber and incubated at 37°C for 35 minutes. The slides were rinsed in distilled water and mounted with glycerine jelly.

2.3.2. Heterocephalus glaber

Tissue preparation and sectioning

The muscles of the fixed *H. glaber* specimens were harvested and processed in an Automated Vacuum Tissue Processor (ASP6025; *Leica Biosystems, Wetzlar, Germany*). The cross-sections of the mid-belly of each muscle were embedded into Paraplast® paraffin wax blocks using a Leica EG 116 Embedder (*Leica Biosystems,*

Wetzlar, Germany) according to the pre-determined slide layout (Figure 1). Each wax block was sectioned using a Leica RM 2125 RT microtome (*Leica Biosystems, Wetzlar, Germany*) to produce three serial sections that were placed onto positively charged slides. Furthermore, three additional muscles (*mm. latissimus dorsi, anconeus* and *flexor carpi ulnaris*) of *B. suillus* were harvested and fixed in 10% buffered formalin for a minimum of 24 hours after which the muscles were processed and embedded into paraffin wax blocks with Paraplast® paraffin wax and a Leica EG 116 Embedder (*Leica Biosystems: Johannesburg, South Africa*). The fixed *B. suillus* muscles were placed into two wax blocks (1-*m. latissimus dorsi;* 2- *mm. flexor carpi ulnaris* and *triceps brachii caput medialis*) and were sectioned onto positively charged slides. These additional three muscles served as a test which compared the staining of the muscle fibres between the fresh and the fixed muscle tissue to ensure the different approaches used on the two species were comparable. In addition, these muscles served as the positive control for the slow MHC staining in the *H. glaber* tissue.

Staining

For the fixed *H. glaber* muscle tissue, antigen retrieval was conducted using heat induced epitope retrieval (HIER) by using an AEG Electrolux Digital Pressure Cooker (*AEG: Frankfurt, Germany*). The prepared slides were first deparaffinised from xylene and rehydrated through a series of ethanols of various concentrations for 10 minutes in each solution. Thereafter, the slides were placed into a metal slide rack and submerged into Leica BOND Epitope Retrieval Solution (X10 concentrate, pH 6; *Leica Biosystems: Wetzlar, Germany*) within the pressure cooker. The slides were steamed on high pressure for one minute after which the steam was released. The slide rack was removed

and placed into a container with warm water (60-80°C) before slowly washing the slides with running tap water. This allowed the slides to gradually cool down to prevent tissue damage. The slow myosin immunohistochemical staining proceeded as described above for the *B. suillus* tissue. For each run, one of the *B. suillus* slides with fixed tissue was stained and used as a positive control.

For the second staining method with the *H. glaber* tissue, Periodic Acid Schiff (PAS) was applied to demonstrate the glucose content within muscle fibres. An amylase digestion was done using Sigma α-amylase type VI-B (CAS: 9000-90-2; *Sigma-Aldrich: Missouri, United States*) to differentiate between glycogen and other structures such as capillaries and polysaccharides within the sarcolemma. The prepared slides were deparaffinised in xylene and through a series of ethanol concentrations for five minutes in each solution. Thereafter, five to eight drops of 0.35% amylase solution were applied to each tissue section and incubated in a plastic humidity chamber at 38°C for 20 minutes (TC2323 SHEL LAB CO_2 Incubator, *Sheldon Manufacturing Inc.: Cornelius, Oregon, United States*). The slides were washed in tap water and stained according to a slightly adjusted PAS stain protocol (Dubowitz & Sewry, 2007). Briefly, slides were placed into Schiff reagent for twenty minutes instead of the usual 15 minutes. Fibres with a high glycogen content stained dark pink and fibres with a low glycogen content stained light pink. For each run, one of the *B. suillus* slides with fixed tissue was stained to compare the results of the PAS stain with the NADH stain.

Visualization and quantification

The slides for both species were scanned using the 40X objective of an Olympus V120-100L slide scanner (*Olympus Corporation, Tokyo, Japan*) at the University of Cape

Town, Pathology Learning Centre. The images had a final resolution of 16µm per pixel. Quantification of the positively stained fibres per muscle cross section and the staining intensity of both the NADH and PAS stains were done using Qupath version 0.2.3 (Bankhead et al., 2017; RRID:SCR_018257). Prior to the analysis of the slow MHC slides, the image type was set to 'Brightfield (H-DAB)', and the stain vectors of each slide were set for the positive and negative cells in the Qupath programme. The percentage of MHC I fibres for each section was determined by using the polygon tool to select the muscle tissue area (folded and longitudinal tissue areas were avoided) and then using the positive cell detection function to determine the positively stained cell percentages. The negative cells or fibres that were not stained positively were considered to be MHC II fibres.

The differences in the oxidative capacity (NADH) between fibre types were quantified by using the polygon tool to select the muscle tissue area and the cell detection function to determine the area for cell classification. Thereafter, the cell intensity threshold setting was used to classify the cells according to its stain intensity based on the three thresholds automatically determined by the Qupath software. The number of cells per threshold was determined with this setting, which were then calculated as the percentage of light, medium and dark fibres per muscle per species. The same method was applied for the quantification of the glycogen content (as a reflection of oxidative capacity) of the PAS stained slides. Both the positive cell detection and cell detection functions had a maximum cell parameter of 25 µm. Due to the cell size of both species being much larger than the maximum cell parameter of Qupath, the software counted every muscle fibre as 2 cells and automatically determined the percentages from the total detections. The exact settings used in the analysis are detailed in the supplementary information.

Optimization for counting the cells of the different stains (NADH and PAS) was done by comparing the results of the three additional fixed *B. suillus* muscles (PAS stain) and the three frozen muscles of the same *B. suillus* specimen (NADH stain).

2.4. Statistical analysis

Descriptive statistics of the percentages of the muscle fibre composition and oxidative capacity were reported per species, which include the means ± SD. Significant differences between the muscles of each species were determined using a one-way analysis of variance (ANOVA). Fischer's Least Significant Difference (LSD) *post-hoc* test was used to determine the p-values. A $p<0.05$ was considered as statistically significant. Statistica 13.5 (*TIBCO software, Palo Alto, California, USA*) was used to create most of the graphs and to perform all statistical analyses. The graphs were created using ggplot2 (Wickham, 2016) in R (R core team).

3. RESULTS

3.1. Muscle architecture comparisons of muscle groups

The results of the ANCOVA analysis including p-values are detailed in Table 2. Both *B. suillus* (mean body mass=798.23g ± 431.67g) and *H. glaber* (mean body mass =40.76g ± 6.6g) had a proximal to distal reduction in muscle mass in the forelimb (Figure 2). The forelimb muscle mass consists of ~75% proximal and ~25% distal muscle mass, where *B. suillus* has slightly more proximal muscle mass compared to *H. glaber* (<1%). Of all the muscle groups studied, in both *B. suillus* and *H. glaber,* the scapular elevators/rotators had the largest percentage muscle mass of the total forelimb muscle mass (28.5% and 29.9%, respectively). The muscle mass percentage of the limb

Table 2: The analysis of covariance (ANCOVA) results of the comparisons of the muscle groups between species.

Muscle group	**Muscle mass (M_m)**			**Fascicle length (L_f)**			**Physiological cross-sectional area (PCSA)**		
	F	**df**	***P***	**F**	**df**	***P***	**F**	**df**	***P***
Head extensors and hyoid bone depressors	0.1	1	0.76	**18.29**	**1**	**p<.01**	0.13	1	0.72
Scapular elevators	0.65	1	0.42	**11.61**	**1**	**p<.01**	0.85	1	0.36
Limb retractors	2.58	1	0.11	**12.79**	**1**	**p<.01**	**4.69**	**1**	**0.03**
Limb protractors	1.61	1	0.21	**21.42**	**1**	**p<.01**	0.91	1	0.35
Elbow extensors	1.5	1	0.23	**25.81**	**1**	**p<.01**	0.00	1	0.95
Elbow flexors	4.67	1	0.06	**7.74**	**1**	**0.02**	**7.12**	**1**	**0.03**
Carpal extensors	2.85	1	0.11	**15.38**	**1**	**p<.01**	3.87	1	0.06
Carpal flexors	3.25	1	0.08	**14.37**	**1**	**p<.01**	4.17	1	0.05
Digital extensors	**0.39**	**1**	**p<0.01**	**20.08**	**1**	**0.01**	0.00	1	0.95
Digital flexors	2.05	1	0.17	**45.87**	**1**	**p<.01**	0.83	1	0.37

Bold text indicates significant results $p<0.05$

retractors (shoulder flexors) was the second largest group in *B. suillus* (24.9%) and *H. glaber*, respectively.

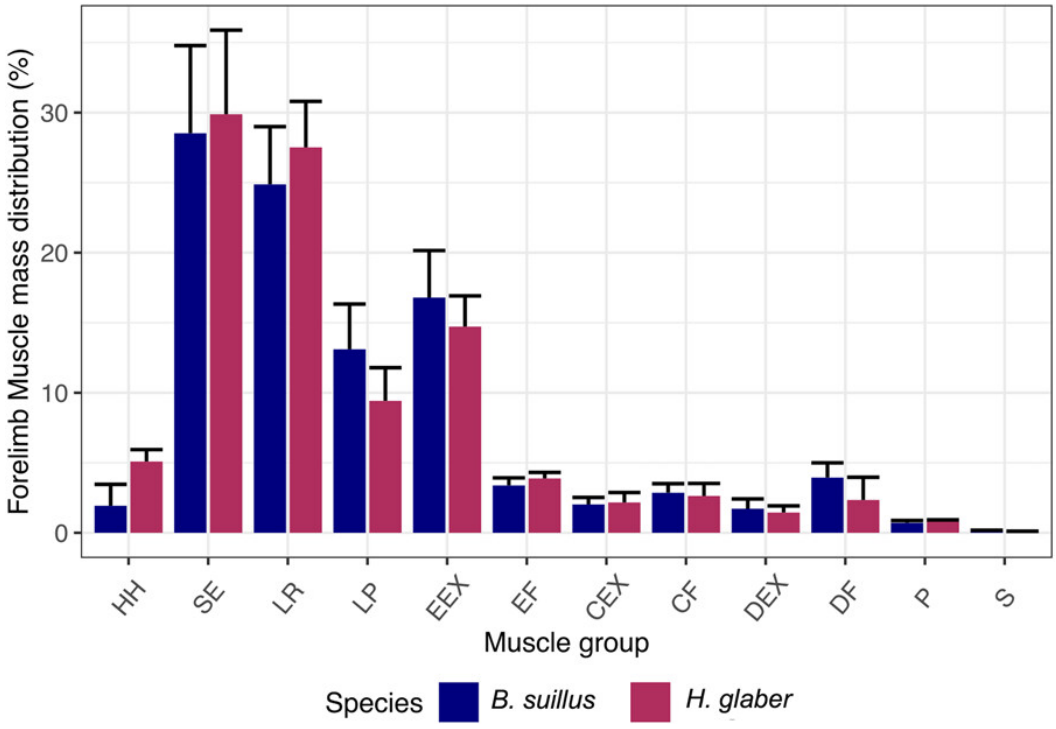

Figure 2. The muscle mass distribution of each muscle group to the total forelimb muscle mass of *Bathyergus suillus* (blue) and *Heterocephalus glaber* (magenta). The summed muscle mass of all the individual muscles was used to calculate the total forelimb muscle mass. Muscle functional group mass is expressed as percentages with the bars indicating the mean percentage of each muscle functional group. See Table 1 for muscle group abbreviations.

Additionally, the fascicles of all the muscle groups were significantly longer in *B. suillus* compared to *H. glaber*. The PCSA values of the limb retractors, elbow flexors, were significantly larger in *B. suillus* compared to *H. glaber* (Table 2).

The mean normalised PCSA of each muscle group was plotted against the mean normalised fascicle length per species illustrated in Figure 3. The scapular elevators and limb retractors of both species are in the upper right quadrant and indicate capabilities of high-power output. The limb protractors of *B. suillus* fall within the upper left quadrant, indicating a slightly higher force capability than the limb protractors of *H. glaber*. Furthermore, the head flexors and hyoid bone depressors (HH) of both species fall within the lower left quadrant. The HH group of *H. glaber* extends further towards the right, which indicates a faster shortening capability via longer fascicles compared to the HH group of *B. suillus*.

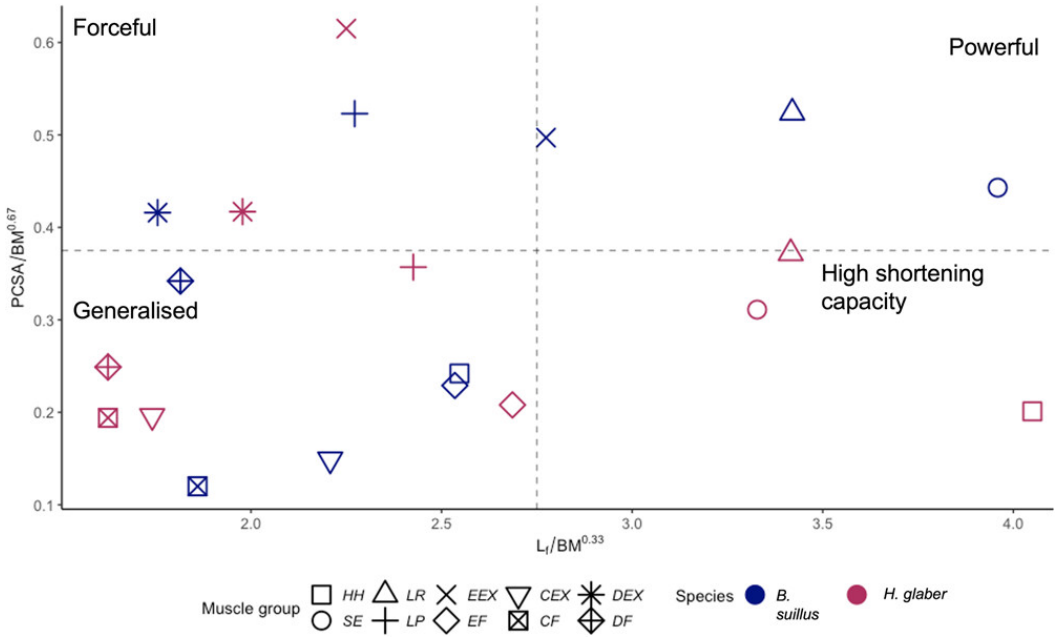

Figure 3. Physiological cross-sectional area (PCSA), normalised to body mass ($PCSA/M_b^{0.67}$) as a function of resting fascicle length normalised to body mass ($L_f/M_b^{0.33}$) of the muscle functional groups in *Bathyergus suillus* (blue) and *Heterocephalus glaber* (magenta). The force capability is represented by the horizontal dashed line (high-above line; low-below line), while the vertical dashed line separates muscles with high (right) and low (left) shortening capability. Muscles located in the upper right quadrant

have both high force and high shortening capabilities and are therefore adapted for high-power outputs. See Table 1 for muscle functional group abbreviations.

3.2. Muscle Architecture Comparison of Individual Muscles

The results of the ANCOVA analysis, including p-values are detailed in Table 3. The values of the measured muscle architecture parameters per species are detailed in Tables 4 and 5.

Significant differences between the two species were found in the normalised muscle mass (M_m) of 21 muscles, with all of these muscles being larger in *B. suillus* compared to those in *H. glaber*. In most of the individual muscles the fascicle lengths were significantly longer in *B. suillus* compared to *H. glaber*. Lastly, the PCSA values of 11 muscles were significantly larger in *B. suillus* compared to *H. glaber*. Additionally, significant differences between *B. suillus* and *H. glaber* were found in the L_f/L_M ratios of *mm. subscapularis* ($p=0.03$), *teres major* ($p=0.01$), *sternocleidomastoideus* ($p=0.04$) and *extensor digitorum communis* ($p<0.01$where *H. glaber* had the larger values (Figure 4). The L_f/L_M ratio of *m. flexor digitorum superficialis* was significantly larger in *B. suillus* compared to *H. glaber* ($p=0.02$; Table 3).

Table 3: The analysis of covariance (ANCOVA) results of the comparisons of the individual muscles between species.

Muscle	**Muscle mass (M_m)**			**Fascicle length (L_f)**			**Physiological cross-sectional area (PCSA)**			**L_f/L_m**		
	F	**df**	***P***	**F**	**df**	***P***	**F**	**df**	***P***	**F**	**df**	***P***
M. Trapezius pars cervicalis	0.21	1	0.66	**26.61**	**1**	**p<.01**	0.35	1	0.57	0.89	1	0.38
M. Trapezius pars thoracis	0.41	1	0.54	**32.6**	**1**	**p<.01**	2.13	1	0.2	0.72	1	0.43
M. Rhomboideus cervicis	0.42	1	0.56	5.82	1	0.09	1.35	1	0.33	2.81	1	0.19
M. Rhomboideus capitis	0.88	1	0.39	5.14	1	0.07	3.91	1	0.1	4.4	1	0.09
M. Serratus ventralis	3.26	1	0.1	**20.62**	**1**	**p<.01**	3.21	1	0.11	0.01	1	0.93
M. Latissimus dorsi	1.26	1	0.29	**8.46**	**1**	**0.02**	0.13	1	0.73	0.06	1	0.81
M. Pectoralis superficialis	0.17	1	0.69	**26.12**	**1**	**p<.01**	0.44	1	0.53	0.2	1	0.67
M. Subclavius	**11.23**	**1**	**0.02**	1.89	1	0.22	**8.46**	**1**	**0.03**	0.01	1	0.92
M. Omotransversarius	0.53	1	0.49	**8.6**	**1**	**0.02**	0.12	1	0.74	1.09	1	0.33
M. Scapuloclavicularis	**7.27**	**1**	**0.02**	**19.65**	**1**	**p<.01**	2	1	0.19	0.29	1	0.6
M. Subscapularis	**15.69**	**1**	**p<.01**	**25.37**	**1**	**p<.01**	4.61	1	0.06	**6.92**	**1**	**0.03**
M. Supraspinatus	**10.35**	**1**	**0.01**	**11.45**	**1**	**0.01**	**6.5**	**1**	**0.03**	5.45	1	0.05
M. Infraspinatus	**22.39**	**1**	**p<.01**	**9.9**	**1**	**0.01**	1.77	1	0.22	0.23	1	0.64
M. Teres major	**5.83**	**1**	**0.04**	4.71	1	0.06	4.48	1	0.06	**12.47**	**1**	**0.01**

Muscle	Muscle mass (M_m)			Fascicle length (L_f)			Physiological cross-sectional area (PCSA)			L_f/L_m		
	F	**df**	***P***	**F**	**df**	***P***	**F**	**df**	***P***	**F**	**df**	***P***
M. Deltoideus pars acromialis	**6.81**	**1**	**0.03**	**92.85**	**1**	**p<.01**	2.92	1	0.12	0.33	1	0.58
M. Deltoideus pars scapularis	**7.21**	**1**	**0.03**	**8.69**	**1**	**0.02**	**10.82**	**1**	**0.01**	4.2	1	0.07
M. Sternohyoideus	0.55	1	0.49	5.19	1	0.07	0.27	1	0.63	0.24	1	0.65
M. Sternoclaviculomastoideus	0.37	1	0.56	**15.22**	**1**	**0.01**	**54.23**	**1**	**p<.01**	**6.6**	**1**	**0.04**
M. Biceps brachii	**11.26**	**1**	**0.01**	**41.25**	**1**	**p<.01**	**23.64**	**1**	**p<.01**	0.38	1	0.55
M. Brachialis	4.67	1	0.06	**7.74**	**1**	**0.02**	**7.12**	**1**	**0.03**	1.89	1	0.2
M. Triceps caput longus	**34.24**	**1**	**p<.01**	**45.19**	**1**	**p<.01**	**20.05**	**1**	**p<.01**	1.15	1	0.31
M. Triceps caput lateralis	**10.12**	**1**	**0.01**	**25.00**	**1**	**p<.01**	0.03	1	0.87	3.74	1	0.09
M. Triceps caput medialis	5.09	1	0.05	**45.45**	**1**	**p<.01**	0.03	1	0.86	3.29	1	0.1
M. Palmaris longus	**6.63**	**1**	**0.04**	1.94	1	0.21	5.9	1	0.05	3.1	1	0.12
M. Pronator teres	**5.5**	**1**	**0.04**	**12.71**	**1**	**0.01**	1.18	1	0.3	0.00	1	0.99
M. Flexor digitorum superficialis	**8.7**	**1**	**0.02**	**33.11**	**1**	**p<.01**	0.17	1	0.69	**9.04**	**1**	**0.02**
M. Flexor digitorum profundus	**12.89**	**1**	**0.01**	**24.97**	**1**	**p<.01**	5.63	1	0.05	0.27	1	0.62
M. Flexor carpi ulnaris	**9.17**	**1**	**0.02**	**13.96**	**1**	**0.01**	**7.16**	**1**	**0.03**	0.42	1	0.54
M. Flexor carpi radialis	**13.8**	**1**	**p<.01**	**6.32**	**1**	**0.03**	**7.16**	**1**	**0.03**	0.18	1	0.68
M. Extensor digiti I longus	**6.08**	**1**	**0.04**	**65.06**	**1**	**p<.01**	2.47	1	0.16	0.13	1	0.73

Muscle	**Muscle mass (M_m)**			**Fascicle length (L_f)**			**Physiological cross-sectional area (PCSA)**			**L_f/L_m**		
	F	**df**	***P***	**F**	**df**	***P***	**F**	**df**	***P***	**F**	**df**	***P***
M. Extensor carpi radialis	**10.04**	**1**	**0.01**	**32.37**	**1**	**p<.01**	4.99	1	0.06	0.02	1	0.9
M. Extensor carpi ulnaris	2.26	1	0.17	**8.13**	**1**	**0.02**	1.71	1	0.22	0.58	1	0.47
M. Extensor digitorum communis	**20.37**	**1**	**p<.01**	**15.45**	**1**	**p<.01**	**22.81**	**1**	**p<.01**	**24.56**	**1**	**p<.01**
M. Extensor digitorum lateralis	**39.06**	**1**	**p<.01**	**11.41**	**1**	**0.01**	**9.22**	**1**	**0.02**	0.01	1	0.93
M. Supinator	3.13	1	0.11	**9.85**	**1**	**0.01**	**12.32**	**1**	**0.01**	0.26	1	0.62

Bold text indicates significant results $p<0.05$

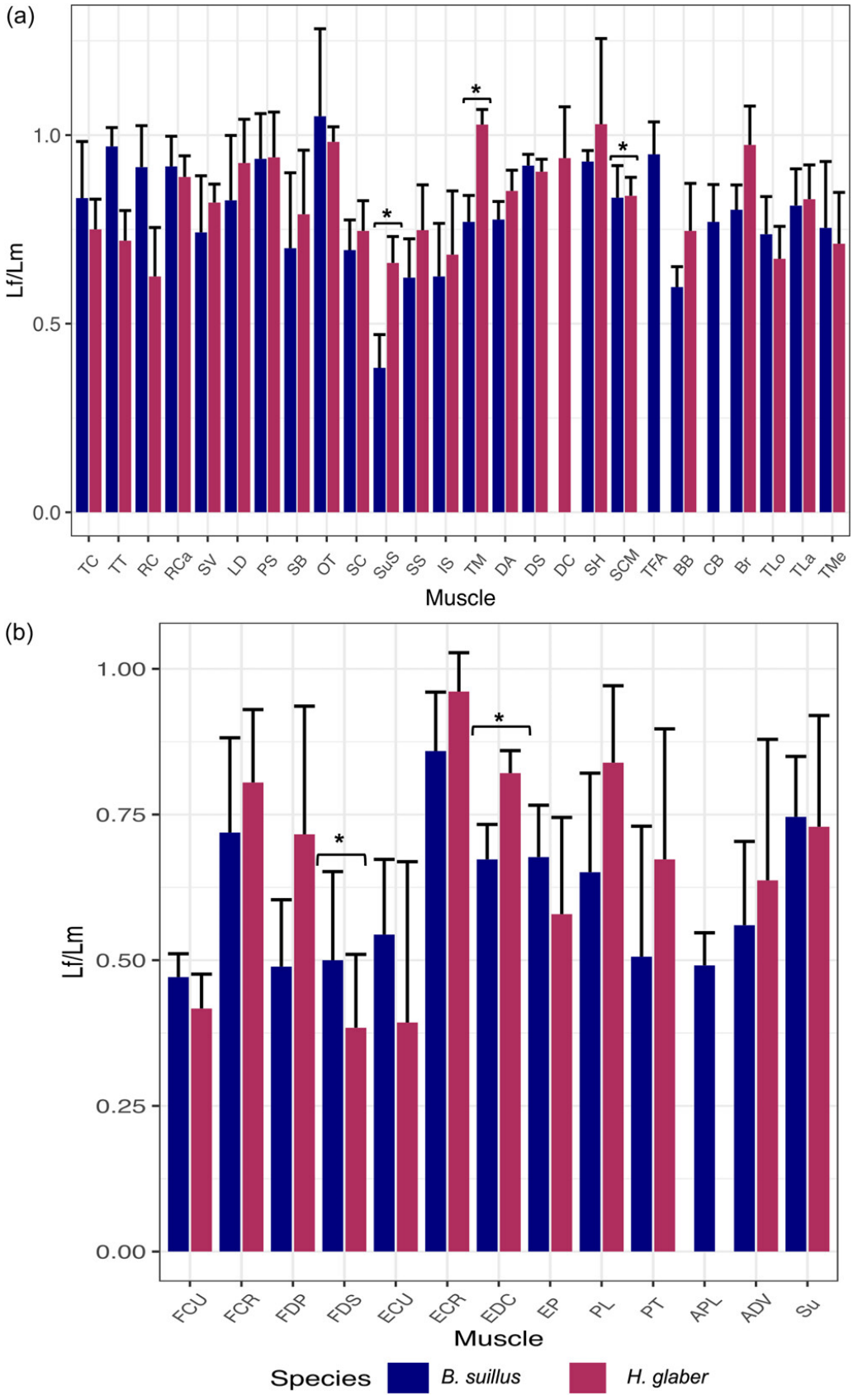
(a)
Lf/Lm
1.0
0.5
0.0
*
*
*
TC
TT
RC
RCa
SV
LD
PS
SB
OT
SC
SuS
SS
IS
TM
DA
DS
DC
SH
SCM
TFA
BB
CB
Br
TLo
TLa
TMe
Muscle
(b)
Lf/Lm
1.00
0.75
0.50
0.25
0.00
*
*
FCU
FCR
FDP
FDS
ECU
ECR
EDC
EP
PL
PT
APL
ADV
Su
Muscle
Species
B. suillus
H. glaber

Figure 4. The mean (±standard deviation) architectural index of muscle fascicle length/muscle belly length (L_f/L_M) for the proximal (a) and distal (b) individual muscles of *Bathyergus suillus* (blue) and *Heterocephalus glaber* (magenta). *Indicates a significant difference of $p < .05$ between species. See Tables 4 and 5 for muscle abbreviations.

The mean normalised PCSA of each individual muscle was plotted against the mean normalised fascicle length per species in Figure 5. The *m. subscapularis* of *B. suillus* is in the highest position in the upper left quadrant, indicating that it produces higher force than *H. glaber*. The *m. latissimus dorsi* of both species is in the lower right quadrant with *H. glaber* having a faster shortening capability than *B. suillus* (far right in lower right quadrant), while that of *B. suillus* has a slightly higher force-output than *H. glaber* (upper right in lower right quadrant). The *m. sternohyoideus* (SH) of *H. glaber* is in the lower right quadrant while the *m. sternocleidomastoideus* is situated to the left of SH. This indicates a higher shortening capacity when compared to the muscles of the HH group (*mm. sternohyoideus* and *sternocleidomastoideus*) of *B. suillus*, which are situated more to the left compared to *H. glaber*.

Table 4: The mean and standard deviation (±) of the architecture parameters of the front limb muscles of *Bathyergus suillus*

Muscle	Abbr.	n	Muscle mass (M_m, g)	Belly length (L_M, mm)	Fascicle length (L_f, mm)	Physiological cross-sectional area (PCSA, mm^2)	Angle of pennation (θ, °)	F_{max} (N)
M. Trapezius pars cervicalis	**TC**	**4**	2.7±1.53	48.90±10.05	36.09±6.01	76.64±51.23	0	22.99±15.37
M. Trapezius pars thoracis	**TT**	**4**	1.21±0.6	67.09±11.33	58.00±10.45	16.99±6.98	0	5.1±2.1
M. Rhomboideus cervicis	**RC**	**3**	0.73±0.39	37.24±12.66	30.29±10.21	22.71±10.4	0	5.11±4.25
M. Rhomboideus capitis	**RCa**	**3**	1.17±0.61	52.92±17.87	42.70±11.5	25.11±8.72	0	5.65±4.33
M. Serratus ventralis	**SV**	**6**	3.35±1.51	51.63±7.79	33.97±5.94	70.91±17.37	48.85±7.55	17.73±9.86
M. Latissimus dorsi	**LD**	**5**	2.33±1.08	74.65±15.88	54.56±12.45	38.72±21.51	24.52±9.5	9.86±7.47
M. Pectoralis superficialis	**PS**	**4**	2.16±0.99	42.08±3.6	35.43±4.92	59.57±27.74	0	14.3±10.76
M. Subclavius	**SB**	**3**	0.09±0.27	19.16±3.66	11.65±0.8	7.01±2.14	0	1.58±1.17
M. Omotransversarius	**OT**	**4**	0.44±0.2	32.96±8.76	30.22±5.88	13.81±5.85	0	3.31±2.4
M. Scapuloclavicularis	**SC**	**6**	0.56±0.22	29.82±4.24	18.75±3.94	29.60±13.46	0	8.88±4.04
M. Subscapularis	**SuS**	**6**	1.69±0.55	36.18±3.38	12.38±2.4	118.57±47.43	31.49±6.99	35.57±14.23
M. Supraspinatus	**SS**	**6**	1.38±0.5	37.40±2.16	20.92±3.55	56.12±19.31	26.37±7.23	16.84±5.79
M. Infraspinatus	**IS**	**6**	1.37±0.47	39.52±2.47	22.32±5.52	57.59±29.25	21.08±3.41	17.28±8.77
M. Teres major	**TM**	**6**	0.61±0.24	34.45±6.85	24.01±6.05	24.85±9.62	0	7.45±2.89
M. Deltoideus pars acromialis	**DA**	**6**	0.48±0.19	23.63±2.43	16.55±2.16	28.79±12.6	0	8.64±3.78

Muscle	Abbr.	n	Muscle mass (M_m, g)	Belly length (L_M, mm)	Fascicle length (L_f, mm)	Physiological cross-sectional area (PCSA, mm^2)	Angle of pennation (θ, °)	F_{max} (N)
M. Deltoideus pars scapularis	**DS**	**6**	0.61±0.24	34.65±5.9	23.74±5.69	24.63±7.29	0	7.39±2.19
M. Sternohyoideus	**SH**	**3**	0.22±0.12	27.25±4.79	22.95±4.4	9.81±6.74	0	1.77±2.15
M. Sternoclaviculomastoideus	**SCM**	**4**	0.72±0.33	27.88±8.99	20.51±5.44	33.25±17.71	20.11±9.02	7.98±6.41
M. Tensor fasciae antebrachii	**TFA**	**6**	0.14±0.05	22.24±2.2	19.00±2.44	6.10±1.87	0	1.83±0.56
M. Biceps brachii	**BB**	**6**	0.33±0.12	33.01±5.2	17.63±1.64	18.22±6.08	0	5.47±1.82
M. Coracobrachialis	**CB**	**6**	0.15±0.07	30.42±8.44	20.97±6.43	6.14±2.5	0	1.84±0.75
M. Brachialis	**Br**	**6**	0.48±0.2	31.49±6.25	22.77±4.9	20.23±7.03	0	6.07±2.11
M. Triceps caput longus	**TLo**	**6**	2.16±0.69	36.28±2.31	24.04±3.2	83.97±24.49	13.78±1.89	25.19±7.35
M. Triceps caput lateralis	**Tla**	**6**	0.99±0.36	34.80±3.95	30.17±13.42	38.53±20.22	0	11.56±6.07
M. Triceps caput medialis	**TMe**	**6**	0.68±0.28	26.63±1.15	18.16±4.72	40.76±24.05	0	12.23±7.21
M. Palmaris longus	**PL**	**6**	0.18±0.06	28.39±5.6	16.74±6	10.44±3.72	19.44±5.05	3.13±1.12
M. Pronator teres	**PT**	**6**	0.17±0.07	23.33±2.94	10.38±3.07	17.73±8.56	0	5.32±2.57
M. Flexor digitorum superficialis	**FDS**	**6**	0.17±0.05	27.89±3.37	12.48±3.9	13.60±6.06	17.72±8.95	4.08±1.82
M. Flexor digitorum profundus	**FDP**	**6**	0.73±0.23	35.59±3.6	15.45±2.6	44.37±16.29	21.91±5.91	13.31±4.89
M. Flexor carpi ulnaris	**FCU**	**6**	0.38±0.14	31.11±4.24	13.29±2.69	25.19±7.56	21.70±8.95	7.56±2.27
M. Flexor carpi radialis	**FCR**	**6**	0.12±0.04	22.21±2.8	14.45±4.03	8.38±2.89	15.16±5.21	2.51±0.87

Muscle	Abbr.	n	Muscle mass (M_m, g)	Belly length (L_M, mm)	Fascicle length (L_f, mm)	Physiological cross-sectional area (PCSA, mm^2)	Angle of pennation (θ, °)	F_{max} (N)
M. Abductor digiti I longus	**APL**	**6**	0.07±0.02	26.63±3.58	11.67±0.96	5.14±1.37	12.12±1.87	1.54±0.41
M. Extensor digiti I longus	**EP**	**6**	0.02±0.01	20.29±1.88	12.38±2	1.75±0.43	14.73±1.95	0.52±0.13
M. Extensor carpi radialis	**ECR**	**6**	0.33±0.12	26.43±3.22	20.68±2.62	14.67±5.24	15.06±3.12	4.40±1.57
M. Extensor carpi ulnaris	**ECU**	**6**	0.16±0.07	29.86±3.75	14.73±4.29	10.01±3.71	13.49±4.17	3.00±1.11
M. Extensor digitorum communis	**EDC**	**6**	0.16±0.04	28.81±3.59	17.57±3.41	8.54±1.82	8.91±2.22	2.56±0.55
M. Extensor digitorum lateralis	**ADV**	**6**	0.13±0.03	28.59±2.24	14.20±2.86	8.72±3.04	13.84±3.07	2.62±0.91
M. Supinator	**Su**	**6**	0.03±0.01	13.98±2.38	9.40±2.24	76.64±1.03	0	0.92±0.31

Table 5: The mean and standard deviation (±) of the architecture parameters of the front limb muscles of *Heterocephalus glaber*

Muscle	Abbr.	n	Muscle mass (M_m, g)	Belly length (L_M, mm)	Fascicle length (L_f, mm)	Physiological cross-sectional area (PCSA, mm^2)	Angle of pennation (θ, °)	F_{max} (N)
M. Trapezius pars cervicalis	**TC**	**6**	0.07±0.081	16.27±1.394	10.95±1.102	6.12±7.705	0	1.84±2.31
M. Trapezius pars thoracis	**TT**	**4**	0.04±0.006	20.79±0.791	13.55±1.382	2.63±0.275	0	0.79±0.08
M. Rhomboideus cervicis	**RC**	**3**	0.02±0.003	14.20±3.314	7.74±0.651	2.00±0.223	0	0.60±0.07
M. Rhomboideus capitis	**RCa**	**5**	0.06±0.008	18.15±2.286	14.52±2.046	4.11±0.689	0	1.23±0.21
M. Serratus ventralis	**SV**	**6**	0.13±0.019	15.52±1.786	11.45±1.043	5.72±0.965	56.77±6.507	1.72±0.26
M. Latissimus dorsi	**LD**	**6**	0.12±0.02	30.13±2.077	25.05±2.874	4.56±1.01	0	1.37±0.3
M. Pectoralis superficialis	**PS**	**6**	0.07±0.014	13.39±1.578	11.26±1.332	5.75±0.877	0	1.73±0.26
M. Subclavius	**SB**	**6**	0.004±0.001	5.38±0.767	5.48±4.12	0.86±0.424	0	0.26±0.13
M. Omotransversarius	**OT**	**6**	0.02±0.002	13.66±1.431	12.10±1.556	1.69±0.327	0	0.51±0.1
M. Scapuloclavicularis	**SC**	**6**	0.03±0.005	11.49±1.302	7.74±1.361	3.63±0.993	0	1.09±0.3
M. Subscapularis	**SuS**	**6**	0.07±0.009	12.14±0.755	7.24±0.973	8.31±0.979	22.78±3.501	2.49±0.29
M. Supraspinatus	**SS**	**5**	0.04±0.008	12.47±1.122	8.47±7.975	4.71±0.749	22.304.647±	1.41±0.23
M. Infraspinatus	**IS**	**6**	0.03±0.007	13.12±0.456	8.07±1.99	4.08±1.367	20.38±2.934	1.22±0.41
M. Teres major	**TM**	**6**	0.03±0.003	11.66±0.967	10.77±0.684	2.51±0.347	0	0.75±0.1
M. Deltoideus pars acromialis	**DA**	**6**	0.01±0.001	6.60±0.695	5.05±0.502	1.88±0.317	0	0.56±0.1

Muscle	Abbr.	n	Muscle mass (M_m, g)	Belly length (L_M, mm)	Fascicle length (L_f, mm)	Physiological cross-sectional area (PCSA, mm^2)	Angle of pennation (θ, °)	F_{max} (N)
M. Deltoideus pars scapularis	**DS**	**6**	0.02±0.004	11.19±0.749	8.02±0.991	2.97±0.551	0	0.89±0.17
M. Deltoideus pars clavicularis	**DC**	**6**	0.02±0.002	10.27±0.464	9.24±0.77	2.13±0.18	0	0.64±0.05
M. Sternohyoideus	**SH**	**5**	0.01±0.003	15.41±2.967	13.83±0.79	1.01±0.227	0	0.30±0.07
M. Sternoclaviculomastoideus	**SCM**	**6**	0.04±0.009	15.71±2.145	11.88±1.78	3.40±0.88	22.65±6.051	1.02±0.26
M. Biceps brachii	**BB**	**6**	0.02±0.002	10.28±0.851	6.92±1.426	2.30±0.628	0	0.69±0.19
M. Brachialis	**Br**	**6**	0.03±0.005	10.96±0.703	9.61±1.176	2.61±0.383	0	0.78±0.12
M. Triceps brachi caput longus	**TLo**	**6**	0.09±0.01	11.27±1.002	6.81±1.013	12.07±1.321	17.61±2.61	3.62±0.4
M. Triceps brachi caput lateralis	**TLa**	**6**	0.05±0.004	10.85±0.922	8.13±1.295	5.59±0.606	0	1.68±0.18
M. Triceps brachi caput medialis	**TMe**	**6**	0.03±0.003	9.27±0.905	5.94±1.149	4.30±0.985	0	1.29±0.3
M. Palmaris longus	**PL**	**4**	0.01±0.001	7.86±0.761	5.90±0.853	1.01±0.25	0	0.30±0.08
M. Pronator teres	**PT**	**6**	0.01±0.001	6.43±0.887	3.76±0.918	1.96±0.859	0	0.59±0.26
M. Flexor digitorum superficialis	**FDS**	**5**	0.01±0.003	11.94±1.423	4.11±1.402	3.08±0.89	29.70±4.715	0.92±0.27
M. Flexor digitorum profundus	**FDP**	**5**	0.02±0.002	9.25±1.638	6.2±1.706	2.67±0.339	19.98±13.848	0.8±0.1
M. Flexor carpi ulnaris	**FCU**	**5**	0.02 ± 0.002	10.70±0.795	4.00±0.46	4.49±0.691	20.40±6.592	1.35±0.21
M. Flexor carpi radialis	**FCR**	**6**	0.005 ± 0.001	7.37±1.383	5.26±0.837	0.88±0.24	13.40±2.951	0.26±0.07
M. Extensor digiti I longus	**EP**	**4**	0.004 ± 0.001	8.58±0.906	4.03±0.581	1.02±0.181	10.71±2.39	0.31±0.05

Muscle	Abbr.	n	Muscle mass (M_m, g)	Belly length (L_M, mm)	Fascicle length (L_f, mm)	Physiological cross-sectional area (PCSA, mm^2)	Angle of pennation (θ, °)	F_{max} (N)
M. Extensor carpi radialis	**ECR**	**5**	0.02 ± 0.002	9.37±0.2	8.12±0.69	1.96±0.201	19.78±3.895	0.59±0.06
M. Extensor carpi ulnaris	**ECU**	**6**	0.01 ± 0.001	9.37±0.654	3.34±1.175	2.57±0.893	19.03±2.766	0.77±0.27
M. Extensor digitorum communis	**EDC**	**6**	0.01 ± 0.002	9.59±0.761	7.08±0.468	1.17±0.216	10.02±2.079	0.35±0.07
M. Extensor digitorum lateralis	**ADV**	**3**	0.01 ± 0.001	9.31±1.015	5.34±2.243	1.00±0.428	12.98±2.589	0.30±0.13
M. Supinator	**Su**	**4**	0.0014 ± 0.001	4.78±0.827	3.12±1.014	0.43±0.162	0	0.13±0.05

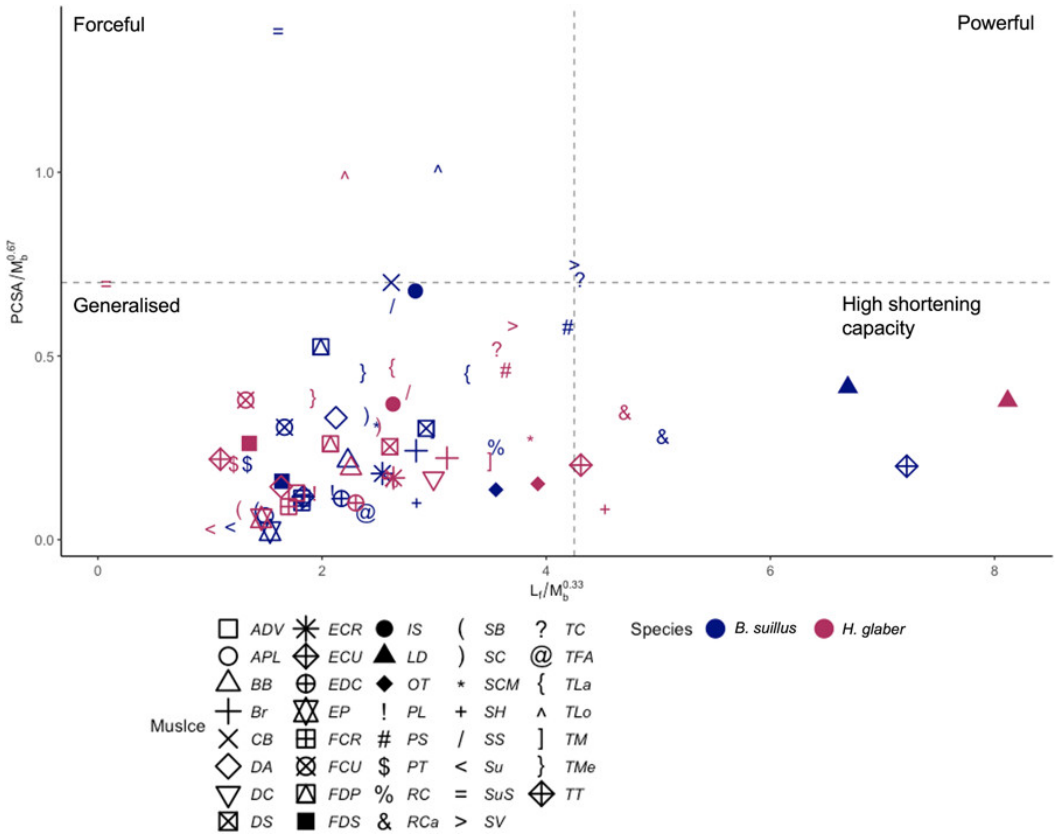

Figure 5. Physiological cross-sectional area (PCSA), normalised to body mass (PCSA/$M_b^{0.67}$) as a function of resting fascicle length normalised to body mass ($L_f/M_b^{0.33}$) of all the individual muscles (*Bathyergus suillus* [blue] and *Heterocephalus glaber* [magenta]). In top panel, the force capability is represented by the horizontal dashed line (high-above line; low-below line), while the vertical dashed line separates muscles with high (right) and low (left) shortening capability. See Tables 4 and 5 for muscle abbreviations

3.3. Muscle fibre typing

3.3.1. Differentiation of type I and II fibres

Both species had predominantly MHC II muscle fibres in all the muscle groups (Figure 6). However, *B. suillus* (mean body mass of 842.79g ± 335.18g) had the least MHC II fibres in all individual muscles when compared to *H. glaber* (mean body mass of 40.76g ± 6.6g), with the exception of *mm. triceps brachii caput lateralis, flexor digitorum*

profundus and *pectoralis superficialis* which had lower MHC II fibre percentages in *H. glaber* (Figure 7).

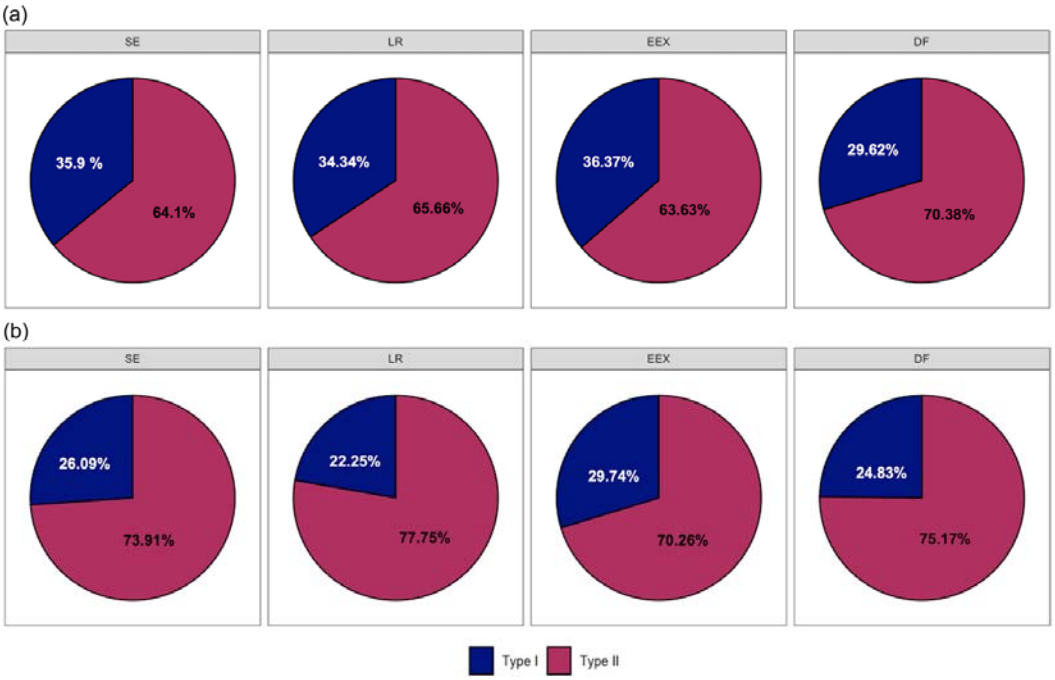

Figure 6. The mean fast and slow myosin heavy chain (MCH) composition (%) of the muscle functional groups in *Bathyergus suillus* (a) and *Heterocephalus glaber* (b). See Table 1 for muscle group abbreviations.

3.

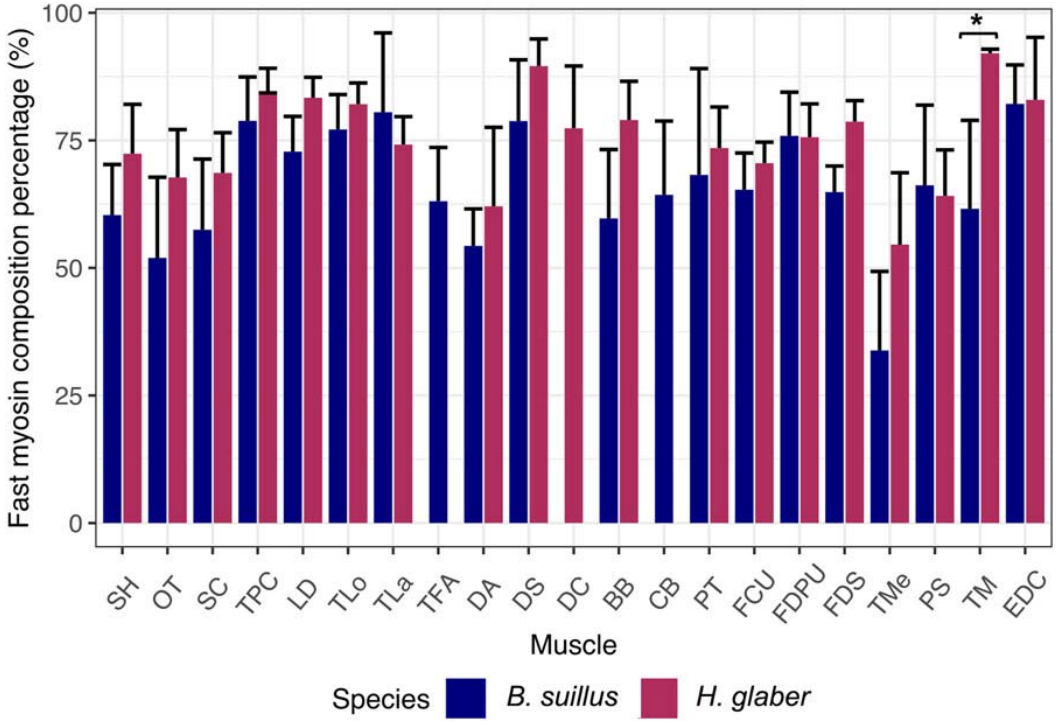

Figure 7. The mean (±standard deviation) of the fast MCH composition (%) of individual muscles in *Bathyergus suillus* (blue) and *Heterocephalus glaber* (magenta). *Indicates statistically significant difference between two species, $p < .05$. See Tables 4 and 5 for muscle abbreviations.

Bathyergus suillus had significantly fewer MHC II fibres in *m. teres major* compared to *H. glaber* (p=0.03; Figure 7). Although not significant, the MHC II fibre percentages in *mm. triceps brachii caput medialis* (TMe) and *biceps brachii* were ±20% lower in *B. suillus* compared to *H. glaber*. Furthermore, TMe in *B. suillus* had the least MHC II fibres (33.8% ± 15.5) while the *m. teres major* in *H. glaber* had the greatest expression of fast fibres (92.1% ± 0.8).

3.3.2. Oxidative capacity

Fibres that had a dark NADH and PAS staining intensity did not necessarily stain positive for slow MHC. Therefore, the fibres that stained positively for slow MHC did not correlate with a high oxidative capacity or glycogen content of fibres (Figure 8). The results from the oxidative, oxidative-glycolytic and glycolytic fibre composition of the NADH and PAS staining were consistent and accurate (Figure 9). Comparison of the frozen NADH and fixed PAS from *B. suillus* tissue sections of *mm. latissimus dorsi,* TMe and *flexor carpi ulnaris* provided results with a difference of less than or equal to ten percent.

The percentage of oxidative fibres in *mm. sternohyoideus, trapezius pars cervicalis* and *flexor digitorum profundus* was significantly higher in *H. glaber* compared to *B. suillus* (Table 6). In contrast, in *B. suillus* the percentage of glycolytic fibres was significantly higher in the *mm. sternohyoideus, scapuloclavicularis, trapezius pars cervicalis, triceps brachii caput longum et lateralis, deltoideus pars scapularis* and *flexor digitorum profundus* compared to the same muscles in *H. glaber* (Table 6). Although not statistically significant, between the two species *m. latissimus dorsi* in *B. suillus* had the most glycolytic fibres (55.6% ± 15.2) while the most oxidative and oxidative glycolytic fibres were observed in *H. glaber* in the *mm. latissimus dorsi* (49.4% ± 23.2) and *scapuloclavicularis* (44.4% ± 8.8), respectively.

Table 6: The mean percentage and standard deviation (±) of the oxidative, oxidative glycolytic and glycolytic stained fibres in the individual muscles of *Bathyergus suillus* and *Heterocephalus glaber*.

Muscle	*Bathyergus suillus*			*Heterocephalus glaber*		
	Glycolytic	**Oxidative glycolytic**	**Oxidative**	**Glycolytic**	**Oxidative glycolytic**	**Oxidative**
M. Sternohyoideus	**23.49 ± 17**	43.17 ± 15.66	**33.34 ± 1.55**	**51.53 ± 12.97**	34.75 ± 9.56	**13.72 ± 12.48**
M. Omotransversarius	36.41 ± 20.17	33.99 ± 3.9	29.59 ± 22.46	46.1 ± 12.19	34.18 ± 6.99	19.71 ± 16.22
M. Scapuloclavicularis	**19.23 ± 15.61**	37.5 ± 12.29	43.27 ± 21.5	**29.86 ± 3.03**	44.43 ± 8.82	25.7 ± 11.35
M. Trapezius pars cervicallis	**13.85 ± 9.46**	33.64 ± 9.74	**52.51 ± 16.57**	**39.04 ± 14.2**	30.46 ± 6.7	**30.5 ± 12.08**
M. Latissimus dorsi	13.63 ± 8.74	30.73 ± 8.36	55.64 ± 15.19	26.81 ± 24.25	23.84 ± 10.35	49.44 ± 23.17
M. Triceps brachi caput longus	**24.84 ± 16.56**	33.52 ± 5.26	41.69 ± 16.17	**38.65 ± 12.79**	38.54 ± 11.95	22.81 ± 7.37
M. Triceps brachi caput lateralis	**24.84 ± 25.55**	28.18 ± 5.55	46.98 ± 26.62	**40.15 ± 12.15**	39.05 ± 10.11	20.8 ± 9.53
M. Tensor fasciae antebrachia	31.9 ± 21.2	28.46 ± 10.3	39.64 ± 23.37	-	-	-
M. Deltoideus pars acromialis	17.56 ± 18.39	33.16 ± 8.07	49.28 ± 17.96	35.39 ± 6.67	32.51 ± 8.19	32.1 ± 8.56
M. Deltoideus pars scapularis	**18.9 ± 16.89**	32.29 ± 3.83	48.82 ± 15	**34.28 ± 11.15**	34.86 ± 8.43	30.86 ± 8.2
M. Deltoideus pars clavicularis	-	-	-	34.46 ± 11.05	35.13 ± 9.53	30.41 ± 12.34
M. Biceps brachii	32.42 ± 20	31.76 ± 12.04	35.82 ± 15.46	36.15 ± 8.06	35.47 ± 6.77	28.38 ± 8.05
M. Coracobrachialis	34.12 ± 23.63	33.85 ± 10.84	32.04 ± 29.35	-	-	-
M. Pronator teres	25.14 ± 6.99	36.25 ± 3.36	38.61 ± 15.86	32.94 ± 13.06	32.41 ± 8.15	34.65 ± 14.13

Muscle	*Bathyergus suillus*			*Heterocephalus glaber*		
	Glycolytic	**Oxidative glycolytic**	**Oxidative**	**Glycolytic**	**Oxidative glycolytic**	**Oxidative**
M. Flexor carpi ulnaris	30.28 ± 2.94	35.83 ± 8.84	33.89 ± 3.19	35.78 ± 11.33	39 ± 5.2	25.22 ± 15.57
M. Flexor digitorum profundus	**10.83 ± 24.93**	38.63 ± 13.39	**50.53 ± 24.94**	**41.18 ± 6.39**	33.68 ± 6.83	**20.04 ± 11**
M. Flexor digitorum superficialis	19.16 ± 9.16	27.94 ± 15.08	52.9 ± 15.55	31.5 ± 7.37	33.65 ± 4.32	34.85 ± 11.12
M. Triceps brachii caput medialis	29.72 ± 15.08	42.03 ± 4.31	28.25 ± 23.48	39.04 ± 9.24	36.74 ± 7.17	24.22 ± 5.44
M. Pectoralis superficialis	19.24 ± 11.67	41.48 ± 18.32	39.28 ± 14.48	34.78 ± 3.7	41.03 ± 5.57	24.19 ± 8.72
M. Teres major	47.54 ± 32.2	35.03 ± 3.53	17.42 ± 13.88	28.65 ± 8.39	33 ± 5.56	38.35 ± 12.17
M. Extensor digitorum communis	29.61 ± 16.14	34.28 ± 3.53	36.10 ± 17.84	37.81 ± 12.43	32.1 ± 8.07	30.09 ± 13.02

Bold text indicates significant results $p<0.05$

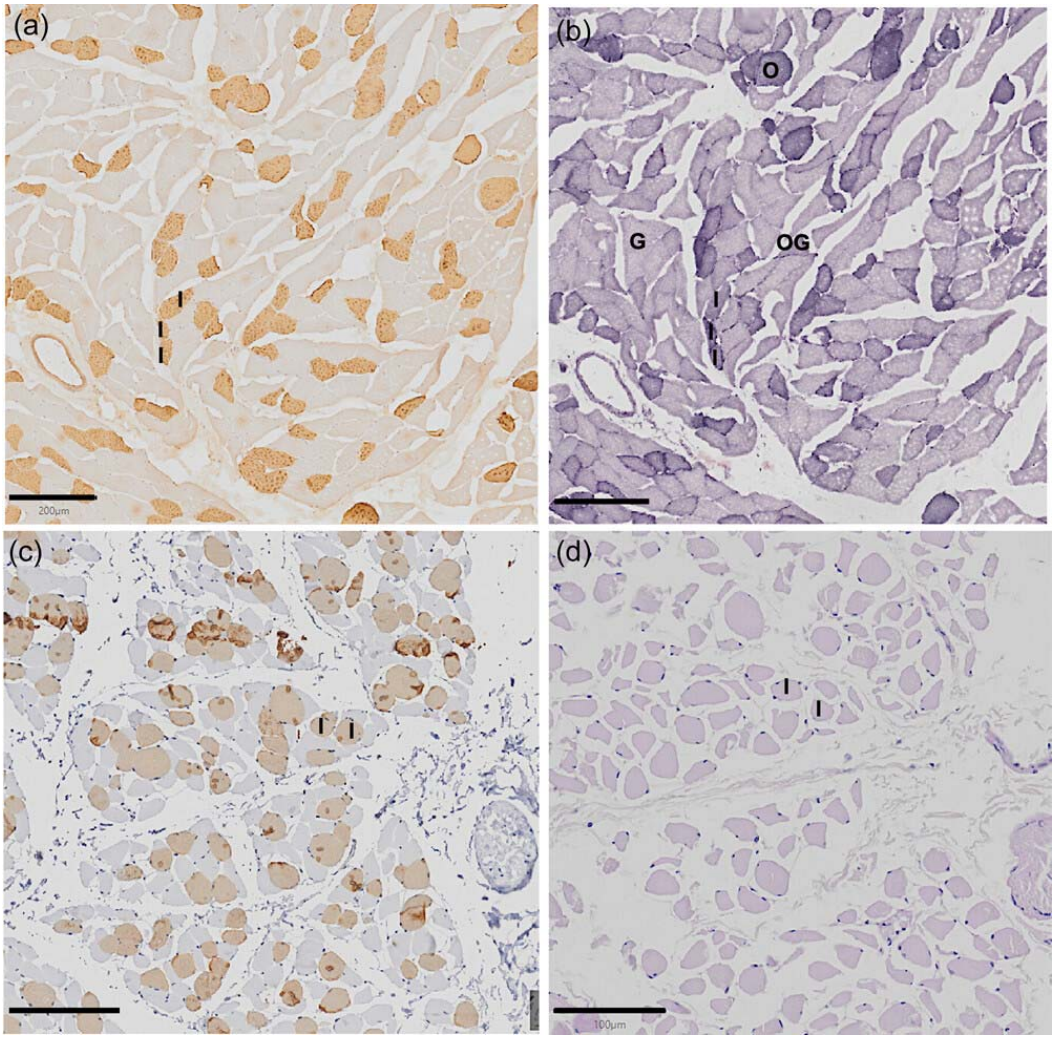

Figure 8. Serial sections of the *m. latissimus dorsi* of *Bathyergus suillus* (a, b) stained for slow myosin heavy chain (MHC-I[a]), NADH (c), slow MHC-I with heat-induced epitope retrieval (c) and Periodic Acid Schiff (PAS) (d). (a, c) The MHC-positive fibres did not necessarily have a high oxidative capacity but were rather stained with a medium to dark intensity (NADH; b) and indistinctly pink stained fibres (PAS; d). MCH-I muscle fibre (I); oxidative fibres (O); oxidative-glycolytic fibres (OG); glycolytic fibres (G). Scale bar: a, b = 200 µm; c, d = 100 µm.

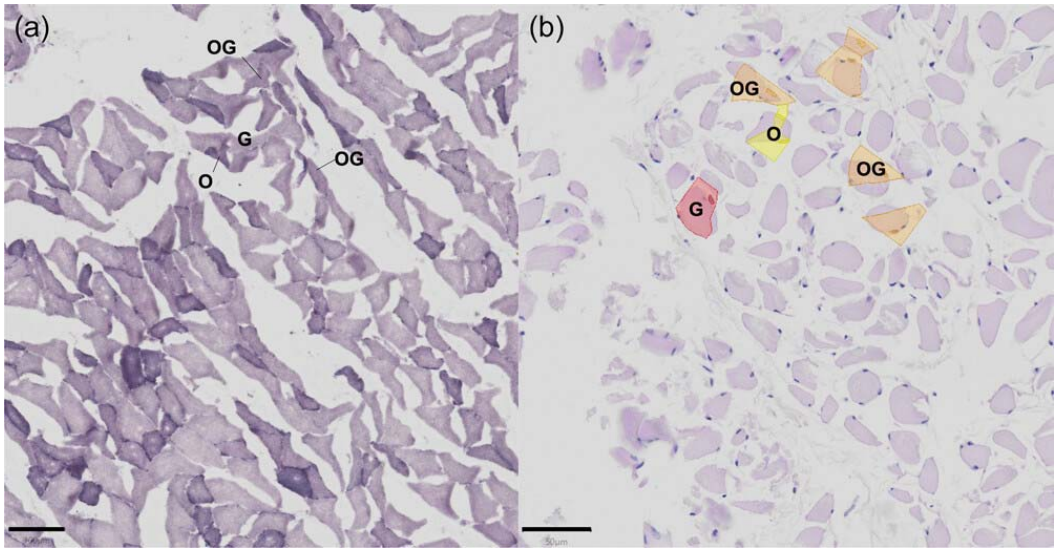

Figure 9. Frozen NADH-stained (a; scale bar = 100 µm) and fixed Periodic Acid Schiff (PAS)-stained (b; scale bar = 50 µm) sections of *m. latissimus dorsi* of *Bathyergus suillus* (a, b). O, oxidative fibres (yellow); OG, oxidative-glycolytic fibres (magenta); G, glycolytic fibres (red).

The mean percentages of the oxidative, oxidative glycolytic and glycolytic fibres in the muscles groups of both species are detailed in Figure 10. The scapular elevators (SE) and digital flexors (DF) had significantly more glycolytic fibres in *B. suillus,* whereas the same two muscle groups (SE and DF) had significantly more oxidative fibres in *H. glaber* ($p = 0.03$). The digital flexors in *B. suillus* had the highest percentage of glycolytic fibres and the elbow extensors in *H. glaber* had the highest percentages of oxidative glycolytic and oxidative fibres.

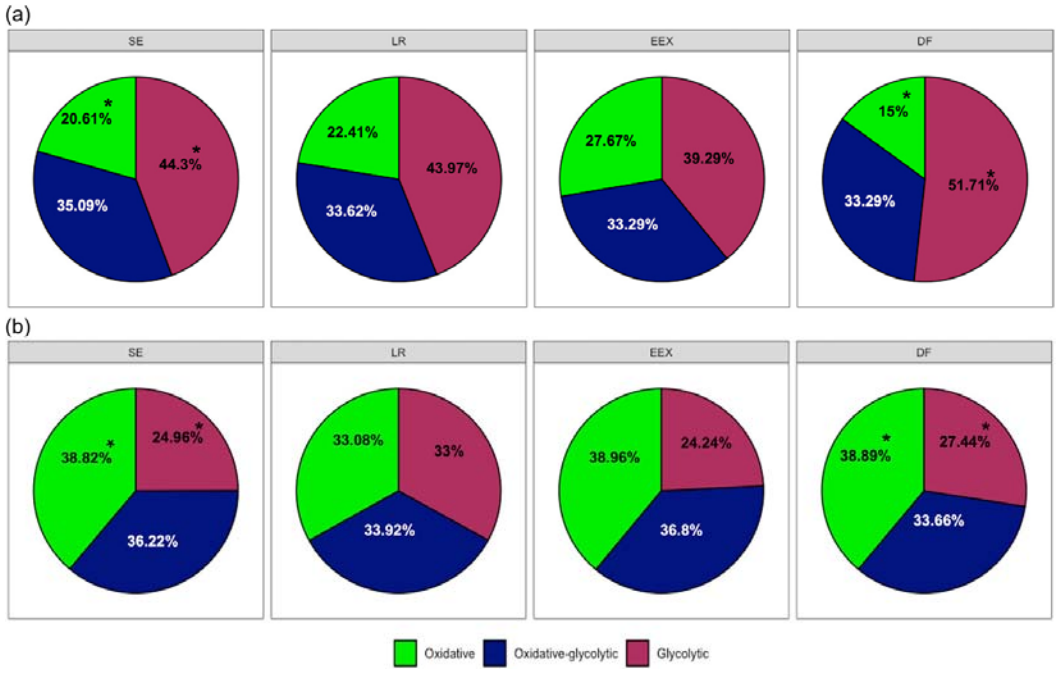

Figure 10. The mean percentages of the oxidative, oxidative-glycolytic and glycolytic fibres in the muscle groups of *Bathyergus suillus* (a) and *Heterocephalus glaber* (b). *Indicates statistically significant difference between two species, $p < .05$. See Table 1 for muscle functional group abbreviations.

4. DISCUSSION

Skeletal muscles produce force dependent on area while velocity of contraction is dependent on length (Lieber & Ward, 2011). Therefore, the integration of muscle architecture parameters and muscle fibre type compositions determined in the current study provide insight into the relationship between homologous muscles and synergistic muscle groups, as well as functional specialisation in the scratch-digging *B. suillus* and chisel-tooth digging *H. glaber*.

In both fossorial mole-rat species studied here, a proximal-to-distal reduction in forelimb muscle mass was observed. This is a feature observed in the forelimbs of highly cursorial mammals such as hares (*Lepus europeus;* Williams, Payne & Wilson, 2007),

cheetahs (*Acinonyx jubatus;* Hudson, Corr, Payne-Davis, Clacy, Lane & Wilson, 2011), greyhounds (*Canis lupus familiaris*; Pasi & Carrier, 2003) and horses (Brown, Kawcak, McIlwraith & Pandy, 2003) as well as the fossorial Eastern mole (*Scalopus aquaticus*; Rose et al., 2013) and several scratch-digging species such as the nine-banded armadillo (*Dasypus novemcinctus,* Olson et al., 2016), ground hog (*Marmota monax,* Rupert et al., 2015), where limb muscle mass is concentrated proximally (Hildebrand & Goslow, 2001). Contrary to this pattern, primates and the arboreal pine marten (*Martes martes*) have greater distal limb mass (approximately 40%; Isler et al., 2006; Raichlen, 2006; Böhmer, Fabre, Herbin, Peigné & Herrel, 2018). This indicates that higher distal limb mass may be advantageous for climbing, object manipulation, whereas high proximal forelimb muscle mass may be an adaptation for running (Böhmer et al., 2018) or burrowing (Olson et al., 2016). Therefore, the limb muscle mass distribution of both *B. suillus* and *H. glaber* (~75% proximally and ~25% distally) may reflect the functional need of fossorial animals to rapidly move bidirectionally within their burrow systems as well as produce the powerful contractions of the limb retractors and scapular elevators during the power stroke (Eilam, Adijes & Vilensky, 1995; Montoya- Sanhueza, Wilson, & Chinsamy, 2019; Montoya-Sanhueza, Šaffa, Šumbera, Chinsamy, Jarvis & Bennett, 2022).

According to Kikuchi (2010), PCSA values typically increase with increasing body mass and since an increase in PCSA was observed in all muscles of *B. suillus,* body mass was used as a covariate to compare the two species. Similar to other scratch-digging mammals (Moore et al., 2013; Rose et al., 2013; Rupert et al., 2015; Olson et al., 2016), the PCSA values of the muscles involved in the power stroke of the scratch-digging animal (limb retractor muscle group, LR) were significantly higher in *B. suillus*

compared to *H. glaber*. In addition to the limb retractors, the scapula elevators / stabilisers (SE) are one of the main muscle groups involved in the power stroke of scratch-digging animals (Martin et al., 2019). Both these muscle groups are indicated in the present study to be powerful, which means they are capable of both fast and forceful contractions. Therefore, in *B. suillus,* although not statistically significant, the slightly higher force output of the LR and slightly higher shortening capacity of the SE (Figure 2) could potentially provide the required power during the power stroke of digging. This feature was also seen in other scratch-digging animals such as the American badger (*Taxidea taxus;* Moore et al., 2013), groundhogs (*Marmota monax,* Rupert et al., 2015) and the nine-banded Armadillo (*Dasypus novemcinctus*; Olson et al., 2016)**.** Furthermore, the fascicle lengths of the major extrinsic muscles involved in scratch-digging, such as the *mm. latissimus dorsi* and *pectoralis major*, were significantly greater in *B. suillus* when compared to *H. glaber,* providing a higher shortening capacity (Table 2 & 3). The longer fascicles allow these extrinsic muscles to retract the forelimb through a large range of motion during the power stroke (Rupert et al., 2015; Martin et al., 2019). However, *H. glaber* also have powerful LR and SE which may indicate a stabilisation function of the shoulder during chisel tooth digging and increase the leverage of the head/neck/jaw to produce enough forward force to bite the soil with their incisors in combination with a downward thrust of the elbow extensors (EEX; Gambarayan & Gasc, 1993; Van Wassenbergh, Heindrycks & Adriaens, 2017; Montoya-Sanhueza et al., 2022) as evidenced by the EEX being capable of forceful contractions (Figure 3).

The *m. subscapularis* (SuS) of *B. suillus* had the highest force output compared to the other muscles in both species. Because SuS had a slow shortening capacity in *B. suillus*

(short fascicle length), the high PCSA and isometric F_{max} of the muscle are responsible for high force production typically seen in scratch-diggers, such as the American badger (*Taxidea taxus;* Moore et al., 2013) and the nine-banded Armadillo (*Dasypus novemcinctus*; Olson et al., 2016). The high force output of the SuS functions to counter the resistance of the soil against limb retraction during scratch-digging (Moore et al., 2013). Furthermore, the high force output of SuS may provide a stabilising function (Moore et al., 2013) to support the larger body mass of *B. suillus* which requires relatively large forces for locomotion, scratch-digging and balance during hind foot drumming (Williams et al., 2007; Lamas, Main & Hutchinson, 2014; Randall, 2014; Martin et al., 2019). This is further supported by the lower percentages of MHC II fibres that were observed in the forelimb muscles of *B. suillus*, when compared to their hind limb muscles (Sahd et al., 2022b).

Architectural indices or L_f/L_M ratios higher than 0.5 indicate that a muscle has a large range of contraction to move over a joint as well as a high muscle shortening capacity-excursion/velocity of contraction (Rose et al., 2013; Rupert et al., 2015; Olson et al., 2016). The L_f/L_M ratios of both *mm. subscapularis* (SuS), *teres major* (TM), as well as *sternocleidomastoideus* (SCM) were significantly smaller in *B. suillus* compared to *H. glaber*. Furthermore, these three muscles (SuS, TM, SCM) had higher force outputs in *B. suillus* compared to *H. glaber* (Figure 5). The low contraction velocity combined with the higher force output of SuS and TM may indicate a stabilisation function of the shoulder joint rather than fast movements in *B. suillus* (von Meiring & Fischer, 1999; Moore et al., 2013). The stabilisation function of the TM muscle is further reflected in the significantly lower percentage of MHC II fibres in *B. suillus* compared to *H. glaber* and may point towards the need for stabilisation of the forelimbs of *B. suillus* during

hind foot drumming and the stabilisation of the shoulder joint during burrowing (Rupert et al., 2015). However, TM has a predominately glycolytic metabolism (47.5%) in *B. suillus* which again indicates the lack of relationship between MCH expression and metabolism (Kohn et al., 2007).

Interestingly, the PCSA value of SCM was significantly higher in *H. glaber* compared to *B. suillus*. Therefore, large values of both the L_f/L_M ratio and PCSA of the SCM seems to be an adaptation for more forceful and faster contralateral movements of the head (Cain, Reynolds & Sarko, 2019) in *H. glaber*. This is reflected in the increased range of motion in the neck allowing the forelimbs and shoulders to remain in a fixed place to produce forward force. Additionally, it could act as a stabilising muscle for anchorage of the upper incisors into the soil during chisel tooth digging (Van Wassenbergh et al., 2017). The SCM of *H. glaber* appears to support its functional requirements for chisel-tooth digging, whereas the slightly larger force output of SCM in *B. suillus* may be contributed to its larger body mass and the need to stabilise and move its large head contralaterally. Although muscle fibre typing was not performed on the SCM, the percentage of oxidative fibres in the *m. sternohyoideus* (SH) of *H. glaber* was significantly higher compared to *B. suillus*. The SH (a head/neck flexor) in *H. glaber* may play a role in endurance movements of the jaw during long periods of digging by stabilising the mandible (as SH inserts on the mandibular symphysis (Doubell et al, 2020)) to allow effective action of the other neck muscles such as the digastric muscle, which retracts the mandible in *H. glaber* (Woods, 1975; Cain et al., 2019). The large muscle mass percentage (Figure 1) and fast shortening capacity (Figure 2) of the head flexor and hyoid bone depressor (HH) muscle group further indicates the

likelihood that the enlarged neck muscles may be an adaptation for chisel-tooth digging in *H. glaber*.

In the current study, the differences observed in the muscle fibre type composition of the forelimb muscles may not be due to functional strains or environmental demands, but rather the phylogeny of the species (Alvarez & Perez, 2019). Ichikawa et al. (2019) discovered the absence of MHC IIb fibres within the muscles of two species of subterranean true moles (Eulipotyphla), whereas all subtypes of fast MHC II fibres were present in the semi-fossorial, terrestrial and semi-aquatic Eulipotyphla species. This suggests that the subterranean habitat may have an influence on the MHC II fibre compositions in species belonging to the same phylogenetic order. Terrestrial animals have to maintain body equilibrium and produce maximum speed to avoid predators or hunt prey, whereas subterranean mammals have no need to support their body weight to move at high speeds (Nevo, 1979). However, the fast movements produced for digging in subterranean mammals may influence the percentages of the subtypes of MHC II fibres, which were not evaluated in the present study. Furthermore, Ichikawa et al. (2019) indicated the absence of MHC I fibres in two subterranean mole species within the order Eulipotyphla (Douady et al., 2002). Other studies performed on species belonging to Eulipotyphla confirmed the absence of slow MHC I fibres within species with different locomotor habits and suggest that it may be due to phylogenetic effects and not locomotor adaptations (Suzuki, 1990; Peters et al., 1999; Savolainen & Vornanen, 1995). Recent studies have placed *H. glaber* into its own separate family, the Heterocephalidae (Patterson & Upham, 2014; Patterson, 2016; Burgin, Colella, Kahn & Uphan, 2018; Tavares & Seuánez, 2018; D'Elía, Fabre, & Lessa, 2019), whereas previously, *B. suillus* and *H. glaber* belonged to the same phylogenetic family,

Bathyergidae. Therefore, even though both of these species inhabit a subterranean environment, differences in muscle characteristics such as the architecture and fibre type composition, may be more attributable to phylogeny and not sociality or digging methods. However, in order to determine if the results herein are phylogenetically driven, further studies need to be conducted that include more species and incorporate a corrective phylogenetic analysis.

Several studies focusing on muscle enzyme activity suggest little correlation between MHC isoform expression and muscle energy metabolism (Kohn, et al., 2011a; Kohn, et al., 2011b; Curry et al., 2012). However, oxidative capacity can be changed in response to environmental and functional stimuli without transformations to the MHC isoform content (Gollnick, Riedy, Quitinskie & Bertocci, 1985). More recently, Bloemberg & Quadrilatero (2012) reported that fast MHC isoforms may have different oxidative capacities across different muscles. Furthermore, other studies have shown the transformation of glycolytic fibres to oxidative fibres in both humans and rodents that underwent endurance training (Yan et al., 2011). This coincides with the observations of the present study as evidenced in Figure 8 where slow MHC-1 I fibres have differing oxidative capacities within the same muscle of *B. suillus* and no difference in oxidative capacity at all between muscle fibres of *H. glaber,* regardless of MHC I expression. Additionally, in the current study, the scapular elevators and digital flexors had significantly higher percentages of glycolytic fibres in *B. suillus* compared to *H. glaber*. This may indicate that various functional demands, such as vigorous bouts of scratch-digging in *B. suillus,* may lead to a transition of oxidative fibres to glycolytic fibres in muscles that are involved in the power-stroke of digging. This transition may be to assist in reducing the bioenergetic cost of burrowing (Lovegrove,1989), by lowering the

amount of oxygen needed for the muscles by relying on the anaerobic processes of glycolytic muscle fibres.

4.1. LIMITATIONS

The current study has several limitations. Information of health status, sex and breeding status was not known for all *B. suillus* specimens. Hormones have a known effect on muscle morphology and fibre type composition (English, Eason, Schwartz, Shirely & Carrasco, 1999; Daniels, Tian & Barton, 2007; Schiaffino & Reggiani, 2011), therefore possibly affecting the results of the present study. On the other hand, the *H. glaber* specimens were all male subordinates and have not gone through sexual maturation, thereby eliminating the effect of hormones on their muscle morphology and fibre type composition (Pinto, Jepsen, Terranova & Buffenstein, 2010). Thus, it is possible that differences in muscle architecture and muscle fibre typing between species, specifically the large standard deviations in the values of *B. suillus,* may have been influenced by sexual dimorphism (Schiaffino & Reggiani, 2011).

The naked mole-rat specimens used were already fixed in 10% buffered formalin, and therefore the staining protocols, and techniques used for fibre typing had to be adapted for fixed tissue for comparison with the fresh-frozen *B. suillus* samples. The NADH stain could only be applied to the fresh-frozen *B. suillus* and was compared to a PAS stain on the *H. glaber* tissue. It is also important to note that this method of determining oxidative capacity is qualitative in nature. Furthermore, the present study did not differentiate between the types of fast fibres.

Furthermore, the limbs of the *H. glaber* and some of the *B. suillus* specimens were not exactly fixed at an angle of 90°, but as close as possible. Due to the relatively small size

of the muscles measured in the present study, the length of the fascicles had to be measured on images rather than on the muscles themselves. Therefore, only superficial fascicles were measured, and this may influence the results of the study as superficial fascicles tend to be longer than those situated more deeply in the muscle (Martin et al., 2019). Both these factors may have influenced the architectural analysis. Additionally, muscle moment arms were not measured in the present study.

5. CONCLUSION

Muscle mass percentage, force output and shortening capacity of muscles involved in the power stroke of scratch-digging, including the limb retractors and digital flexors, were all greater in *B. suillus* compared to *H. glaber*, and may reflect adaptations for scratch-digging in the forelimbs of *B. suillus*. The muscle architecture and fibre type compositions of the neck muscles in *H. glaber* suggest adaptations for chisel-tooth digging.

Although myosin heavy chain (MHC)-expression of muscle fibres are possibly not strongly influenced by functional and environmental strains, metabolic transformation of oxidative and glycolytic fibres may take place due to functional strains (Glaser et al., 2009; Yan et al., 2011). Significantly higher glycolytic fibres in the scapular elevators and digital flexors in *B. suillus* may be a result of the functional demands of vigorous scratch-digging (or the expression of MHC-IIA and IIX fibres) and not phylogeny as these mentioned muscle groups are particularly active during scratch-digging (Rupert et al., 2015).

There are multiple aspects of the muscle architecture and fibre type compositions in the forelimb muscles of *B. suillus* that reflect possible adaptations for scratch-digging

and hind foot-drumming. However, the possibility remains that these differences may be attributed to phylogeny. Future research can be performed on other African mole-rat species that are closely related to *B. suillus* and *H. glaber* respectively to provide further insight on the effect of phylogeny on the muscle structure in this rodent family.

ACKNOWLEDGEMENTS

The authors would like to thank Prof Martin Kidd for assistance with the statistical analysis and Mr Reggie Williams for histology technical assistance. The financial assistance of the National Research Foundation (NRF; Grant number: 120827) towards this research is acknowledged. Opinions expressed and conclusions arrived at are those of the authors and are not necessarily to be attributed to the NRF. The current address for Lauren Sahd is Evolutionary Developmental Biology Research Group, Department of Biology, Ghent University, Ghent 9000, Belgium.

AUTHOR CONTRIBUTIONS

Lauren Sahd assisted with the muscle harvesting and histological staining, aided with analysis and revised the manuscript. Narusa Doubell performed the histological staining and analysis and drafted the original manuscript. Nigel Bennett provided samples and contributed to manuscript drafts. Sanet Kotzé designed the project, provided funding and samples and edited the manuscript.

REFERENCES

Acevedo, L. M. & Rivero, J. L. (2006). New insights into skeletal muscle fibre types in the dog with particular focus towards hybrid myosin phenotypes. *Cell and Tissue Research*, 323: 283–303. https://doi.org/10.1007/s00441-005-0057-4

Álvarez, A. & Pérez, M. (2019). Deep changes in masticatory patterns and masseteric musculature configurations accompanied the eco-morphological evolution of cavioid rodents (Hystricognathi, Caviomorpha). *Mammalian Biology* 96: 53–60. https://doi.org/10.1016/j.mambio.2019.03.009

Bankhead, P., Loughrey, M. B., Fernández, J. A., Dombrowski, Y., McArt, D. G., Dunne, P. D., ... & Hamilton, P. W. (2017). QuPath: Open source software for digital pathology image analysis. *Scientific reports* 7: 1-7. https://doi.org/10.1038/s41598-017-17204-50

Bennett, N. C. & Faulkes, C. G. (2000). African mole-rats: ecology and eusociality. Cambridge University Press, United Kingdom.

Bennett, N. C. & Jarvis, J. U. M. (1988). The reproductive biology of the Cape mole-rat, *Georychus capensis* (Rodentia, Bathyergidae). *Journal of Zoology* 214 95–106. https://doi.org/10.1111/j.1469-7998.1988.tb04989.x

Bloemberg D & Quadrilatero J. (2012). Rapid determination of myosin heavy chain expression in rat, mouse, and human skeletal muscle using multicolor immunofluorescence analysis. *PLoS ONE* 7:e35273. doi: 10.1371/journal.pone.0035273

Bodine, S. C., Roy, R. R., Meadows, D. A., Zernicke, R. F., Sacks, R. D., Fournier, M. & Edgerton, V. R. (1982). Architectural, histochemical, and contractile characteristics of a unique biarticular muscle: the cat semitendinosus. *Journal of Neurophysiology* 48: 192–201. https://doi.org/10.1152/jn.1982.48.1.192

Böhmer, C., Fabre, A. C., Herbin, M., Peigné, S. & Herrel, A. (2018). Anatomical basis of differences in locomotor behaviour in martens: A comparison of the forelimb musculature between two sympatric species of Martes. *The Anatomical Record*, 301: 449–472. https://doi.org/10.1002/ar.23742

Brett, R. A. (1991). The population structure of naked mole-rat colonies. In P.W. Sherman, J.U.M. Jarvis, and R.D. Alexander (eds.), *The biology of the naked mole-rat,* pp. 97-136. Princeton Univ. Press, Princeton.

Brown, N., Kawcak, C.E., McIlwraith, C.W., Pandy, M. (2003) Architectural properties of distal forelimb muscles in horses, *Equus caballus*. *Journal of Morphology* 258:106–114. https://doi.org/10.1002/jmor.10113

Burgin, C.J., Colella J.P., Kahn P.L., Upham, N.S. (2018) How many species of mammals are there? *Journal of Mammalogy* 99: 1-4. https://doi.org/10.1093/jmammal/gyx147

Cain, B.W., Reynolds, T. & Sarko, D.K. (2019) Superficial, suprahyoid, and infrahyoid neck musculature in naked mole-rats (*Heterocephalus glaber*): Relative size and potential contributions to independent movement of the lower incisors. *Journal of morphology*, 280: 1185-1196. https://doi.org/10.1002/jmor.21022

Charles, J.P., Cappellari, O., Spence, A.J., Hutchinson, J.R. & Wells, D.J. (2016) Musculoskeletal geometry, muscle architecture and functional specialisations of the mouse hindlimb. *PLoS One* 11: e0147669. https://doi.org/10.1371/journal.pone.0147669

Curry JW, Hohl R, Noakes TD & Kohn TA. (2012). High oxidative capacity and type IIx fibre content in springbok and fallow deer skeletal muscle suggest fast sprinters with a resistance to fatigue. *Journal of Experimental Biology* 215: 3997-4005 doi: 10.1242/jeb.073684

D'Elía, G., Fabre, P.H. & Lessa, E.P. (2019) Rodent systematics in an age of discovery: recent advances and prospects. *Journal of Mammalogy*, 100: 852-871. https://doi.org/10.1093/jmammal/gyy179

Daniels, D.W., Tian, Z. & Barton, E.R. (2008) Sexual dimorphism of murine masticatory muscle function. *Archives of Oral Biology*. 53: 187-92. https://doi.org/10.1016/j.archoralbio.2007.09.006

Douady, C.J., Chatelier, P.I., Madsen, O., de Jong, W.W., Catzeflis, F., Springer, M.S. & Stanhope, M.J. (2002) Molecular phylogenetic evidence confirming the Eulipotyphla concept and in support of hedgehogs as the sister group to shrews. *Molecular Phylogenetics and Evolution*, 25: 200-209. https://doi.org/10.1016/S1055-7903(02)00232-4

Doubell, N.S., Sahd, L. & Kotzé, S.H. (2020). Comparative forelimb morphology of scratch-digging and chisel-tooth digging African mole-rat species. *Journal of Morphology* 281(9): 1029-1046. https://doi.org/10.1002/jmor.21229

Dubowitz, V. & Sewry, C.A. (2007). *Muscle biopsy- a practical approach.* Philadelphia, Saunders.

Eilam, D., Adijes, M. & Vilensky, J. (1995). Uphill locomotion in mole rats: a possible advantage of backward locomotion. *Physiology & Behaviour.* 58: 483–489.

Eng, C.M., Smallwood, L.H., Rainiero, M.P., Lahey, M., Ward, S.R, & Lieber, R.L. (2008) Scaling of muscle architecture and fiber types in the rat hindlimb. *Journal of Experimental Biology* 211: 2336–2345 https://doi.org/10.1242/jeb.017640

English, A.W., Eason, J., Schwartz, G., Shirley, A. & Carrasco, D.I. (1999) Sexual dimorphism in the rabbit masseter muscle: myosin heavy chain composition of neuromuscular compartments. *Cells Tissues Organs*; 164:179–91. https://doi.org/10.1159/000016658

Fransescoli, G. (2000) Sensory capabilities and communication in subterranean rodents. In: E.A. Lacey, J.L. Patton & G.N. Cameron (eds.). Life Underground: The Biology of Subterranean Rodents, Chicago, USA. The University of Chicago Press. pp. 111-144.

Fukunaga, T., Roy, R.R., Shellock, F.G., Hodgson, J.A. & Edgerton, V.R. (1996) Specific tension of human plantar flexors and dorsiflexors. *Journal of Applied Physiology* 80: 158–65. https://doi.org/10.1152/jappl.1996.80.1.158

Gambaryan, P. P. & Gasc, J.-P. (1993). Adaptive properties of the musculoskeletal system in the mole-rat *Myospalax myospalax* (Marnmalia, Rodentia), cinefluorographical, anatomical and biomechanical analyses of the burrowing. *Zoologische Jahrbücher. Abteilung für Anatomie* 123: 363–401.

Gans, C. & Bock, W.J. (1965) The functional significance of muscle architecture: a theoretical analysis. *Advances in Anatomy, Embryology and Cell Biology* 38: 115–142.

Gans, C. & De Vries, F. (1987) Functional bases of fiber length and angulation in muscle. *Journal of Morphology,* 192: 63–85. https://doi.org/10.1002/jmor.1051920106m

Glaser, B.W., You, G., Zhang, M. & Medler, S. (2010) Relative proportions of hybrid fibres are unaffected by 6 weeks of running exercise in mouse skeletal muscles. *Experimental Physiology*. 95:211-21. https://doi.org/10.1113/expphysiol.2009.049023

Gollnick, P.D., Riedy, M.D., Quintinskie, J.J. & Bertocci, L. (1985). Differences in metabolic potential of skeletal muscle fibres and their significance for metabolic control. *Journal of Experimental Biology* 115:191-9

Hart, L., O'Riain, M.J., Jarvis, J.U.M. & Bennett, N.C. (2006) The pituitary potential for opportunistic breeding in the Cape dune mole-rat, *Bathyergus suillus*. *Physiology & Behaviour* 88: 615–619. https://doi.org/10.1016/j.physbeh.2006.05.020

Hildebrand, M. (1985) Digging of quadrupeds. In: Hildebrand, M., Bramble, D.M., Liem, K.F. & Wake, D.B. (eds), Functional Vertebrate Morphology. Cambridge: Belknap Press of Harvard University. pp. 90–108

Hildebrand, M. & Goslow, G.E. (2001) Digging, and crawling without appendages. In: McFadden, P. (ed.), pp 455–474. Analysis of Vertebrate Structure. New York: Wiley.

Honeycutt, R.L., Allard, M.W., Edwards, S.V. & Schlitter, D.A. (1991) Systematics and evolution of the family Bathyergidae. In Sherman, P.W., Jarvis, J.U.M. & Alexander, R.D. (eds.), *The Biology of the Naked Molerat.* New Jersey, Princeton University Press, pp. 45-65.

Hudson, P.E., Corr, S.A., Payne-Davis, R.C., Clancy, S.N., Lane, E. & Wilson, A.M. (2011) Functional anatomy of the cheetah (*Acinonyx jubatus*) forelimb. *Journal of Anatomy* 218: 375–385. https://doi.org/10.1152/jn.1987.57.2.554

Hyatt, J.P., Roy, R.R., Rugg, S. & Talmadge, R.J. (2010) Myosin heavy chain composition of tiger (*Panthera tigris*) and cheetah (*Acinonyx jubatus*) hindlimb muscles. *Journal of Experimental Zoology* Part A: Ecological Genetics and Physiology 313: 45-57. https://doi.org/10.1002/jez.574

Ichikawa, H., Matsuo, T., Higurashi, Y., Nagahisa, H., Miyata, H., Sugiura, T. & Wada, N. (2019) Characteristics of muscle fibre type distribution in moles. *Anatomical Record* 302: 1010-1023.

Isler, K., Payne, R.C., Gunther, M.M., Thorpe, S.K., Li, Y., Savage, R. & Crompton, R.H. (2006) Inertial properties of hominoid limb segments. *Journal of Anatomy* 209:201–218. https://doi.org/10.1111/j.1469-7580.2006.00588.x

Jarvis, J.U.M. & Sale, J.B. (1971) Burrowing and burrow patterns of East African mole-rats *Tachyoryctes, Heliophobius* and *Heterocephalus*. *Journal of Zoology*. 163: 451-79. https://doi.org/10.1111/j.1469-7998.1971.tb04544.x

Kalmar, B., Blanco, G. & Greensmith, L. (2012) Determination of muscle fiber type in rodents. *Current Protocols in Mouse Biology* 2: 231-243. https://doi.org/10.1002/9780470942390.mo110229

Kikuchi, Y. (2010) Comparative analysis of muscle architecture in primate arm and forearm. *Anatomia, Histologia, Embryologia* 39: 93–106. https://doi.org/10.1111/j.1439-0264.2009.00986.x

Kikuchi, Y. & Kuraoka, A. (2014) Differences in muscle dimensional parameters between non-formalin-fixed (freeze-thawed) and formalin-fixed specimen in gorilla (*Gorilla gorilla*). *Mammalian Study* 39: 65-72. https://doi.org/10.3106/041.039.0101

Kohn TA, Burroughs R, Hartman MJ, Noakes TD. (2011). Fiber type and metabolic characteristics of lion (*Panthera leo*), caracal (*Caracal caracal)* and human skeletal muscle. *Comparative Biochemistry, Physiology and Molecular Integrative Physiology* 159: 125-133.

Kohn TA, Curry JW, Noakes TD. (2011) Black wildebeest skeletal muscle exhibits high oxidative capacity and a high proportion of type IIx fibres. *Journal of Experimental Biology* 214: 4041-7.

Kohn, T.A., Hoffman, L.C. & Myburgh, K.H. (2007) Identification of myosin heavy chain isoforms in skeletal muscle in four southern African wild ruminants. *Comparative Biochemistry and Physiology*, 148: 399–407.

Kubiak, B.B., Maestri, R., de Almeida, T.S., Borges, L.R., Galiano, D., Fornel, R. & De Freitas, T.R. (2018) Evolution in action: soil hardness influences morphology in a

subterranean rodent (Rodentia: Ctenomyidae). *Biological Journal of the Linnean Society*. 26;125(4):766-76. https://doi.org/10.1093/biolinnean/bly144

Kutsukake, N., Inada, M., Sakamoto, S.H. & Okanoya, K. Behavioural interference among eusocial naked mole rats during work. *Journal of Ethology* **37,** 101–109 (2019). https://doi.org/10.1007/s10164-018-0581-9

Lamas, L.P., Main, R.P. & Hutchinson, J.R. (2014) Ontogenetic scaling patterns and functional anatomy of the pelvic limb musculature in emus (*Dromaius novaehollandiae*). *PeerJ*, 2: e716. https://doi.org/10.7717/peerj.716

Lehmann, W.H. (1963) The forelimb architecture of some fossorial rodents. *Journal of Morphology*. 113: 59-76.

Lessa, E.P., Vassallo, A.I., Verzi, D.H. & Mora, M.S. (2008) Evolution of morphological adaptations for digging in living and extinct ctenomyid and octodontid rodents. *Biological Journal of the Linnean Society* 95: 267–283. https://doi.org/10.1111/j.1095-8312.2008.01057.x

Lieber, R.L. & Fridén, J. (2000) Functional and clinical significance of skeletal muscle architecture. *Muscle & Nerve* 23: 1647-1666. https://doi.org/10.1002/1097-4598(200011)23:11<1647::AID-MUS1>3.0.CO;2-M

Lieber, R.L. & Ward, S.R. (2011) Skeletal muscle design to meet functional demands. *Philosophical Transactions of the Royal Society B* 366: 1466-1476. https://doi.org/10.1098/rstb.2010.0316

Lovegrove, B.G. 1989. The cost of burrowing by the social mole rats (Bathyergidae) *Cryptomys damarensis* and *Heterocephalus glaber*: the role of soil moisture. *Physiological Zoology* 62: 449-469.

Martin, M.L., Warbouton, N.M., Travouillon, K.J. & Fleming, P.A. (2019) Mechanical similarity across ontogeny of digging muscles in an Australian marsupial (*Isoodon fusciventer*). *Journal of Morphology* 280: 423-435. https://doi.org/10.1002/jmor.20954

Medler, S. (2002) Comparative trends in shortening velocity and force production in skeletal muscle. *American Journal of Physiology- Regulatory Integrative Comparative Physiology* 283: R368-R378

Mendez, J. & Keyes, A. (1960) Density and composition of mammalian muscle. *Metabolism* 9:184–188.

Montoya-Sanhueza, G., Šaffa, G., Šumbera, R., Chinsamy, A., Jarvis, J. U. M. &Bennett, N. C. (2022). Fossorial adaptations in African mole-rats (Bathyergidae) and the unique appendicular phenotype of naked mole-rats. *Communications Biology* 5: 526. https://doi.org/10.1038/s42003-022-03480-z

Montoya-Sanhueza, G., Wilson L. A. B. & Chinsamy A. (2019). Postnatal development of the largest subterranean mammal (*Bathyergus suillus*): morphology, osteogenesis, and modularity of the appendicular skeleton. *Developmental Dynamics* 248: 1101–1128.

Moore, A.L., Budny, J.E., Russell, A.P. & Butcher, M.T. (2013) Architectural specialisation of the intrinsic thoracic limb musculature of the American badger (*Taxidea taxus*). *Journal of Morphology* 274:35-48. https://doi.org/10.1002/jmor.20074

Nevo, E. (1979) Adaptive convergence and divergence of subterranean mammals. *Annual review of ecology and systematics*, 10: 269-308. https://doi.org/10.1146/annurev.es.10.110179.001413

Olson, R.A., Womble, M.D., Thomas, D.R., Glenn, Z.D. & Butcher, M.T. (2016) Functional morphology of the forelimb of the nine-banded armadillo (*Dasypus novemcinctus*): Comparative perspectives on the myology of Dasypodidae. *Journal of Mammalian Evolution*. 23:49-69. https://doi.org/10.1007/s10914-015-9299-4

Pasi, B.M. & Carrier, D.R. (2003) Functional trade-offs in the limb muscles of dogs selected for running vs. fighting. *Journal of Evolutionary Biology* 16: 324-332. https://doi.org/10.1046/j.1420-9101.2003.00512.x

Patterson, B.D. (2016) Family Heterocephalidae (naked mole-rats). Handbook of mammals of the world.:342-51.

Patterson, B.D. & Upham, N.S. (2014) A newly recognized family from the Horn of Africa, the Heterocephalidae (Rodentia: Ctenohystrica). *Zoological Journal of the Linnean Society* 172: 942-963. https://doi.org/10.1111/zoj.12201

Payne, R.C., Hutchinson, J.R., Robilliard, J.J., Smith, N.C. & Wilson, A.M. (2005) Functional specialization of pelvic limb anatomy in horses (*Equus caballus*). *Journal of Anatomy* 206: 557–574. https://doi.org/10.1111/j.1469-7580.2005.00420.x

Pepper, J.W., Braude, S.H., Lacey, E.A. & Sherman, P.W. (1991) Vocalizations of the naked mole rat. In P.W. Sherman, J.U. M. Jarvis, and R.D. Alexander (eds.), The biology of the naked mole-rat, pp. 243–274. Princeton Univ. Press, Princeton.

Peter, J.B., Barnard, R.J., Edgerton, V.R., Gillespie, C.A. & Stempel, K.E. (1972) Metabolic profiles on three fiber types of skeletal muscle in guinea pigs and rabbits. *Biochemistry* 11: 2627-2733.

Peters, T., Kubis, H.P., Wetzel, P., Sender, S., Asmussen, G., Fons, R. & Jürgens, K.D. (1999) Contraction parameters, myosin composition and metabolic enzymes of the skeletal muscles of the Etruscan shrew *Suncus etruscus* and of the common European white-toothed shrew *Crocidura russula* (Insectivora: soricidae). *Journal of Experimental Biology* 202: 2461–2473. https://doi.org/10.1242/jeb.202.18.2461

Pinto, M., Jepsen, K.J., Terranova, C.J. & Buffenstein, R. (2010) Lack of sexual dimorphism in femora of the eusocial and hypogonadic naked mole-rat: a novel animal model for the study of delayed puberty on the skeletal system. *Bone*. 146:112-20. https://doi.org/10.1016/j.bone.2009.08.060

R Core Team (2013) R: A language and environment for statistical computing. R Foundation for Statistical Computing, Vienna. URL http://www.R-project.org/

Raichlen, D.A. (2006) Effects of limb mass distribution on mechanical power outputs during quadrupedalism. *Journal of Experimental Biology*. 209: 633-644. https://doi.org/10.1242/jeb.02061

Randall, J.A. (2014) Vibrational communication: spiders to kangaroo rats. In: Witzany G (ed) Biocommunication of Animals. Springer, Dordrecht, pp103-133

Rivero, J.L. (2018) Locomotor muscle fibre heterogeneity and metabolism in the fastest large-bodied rorqual: the fin whale (*Balaenoptera physalus*). *Journal of Experimental Biology*. 221 jeb177758 https://doi.org/10.1242/jeb.177758

Rose, J.A., Sandefur, M., Huskey, S., Demler, J.L. & Butcher, M.T. (2013) Muscle architecture and out-force potential of the thoracic limb in the eastern mole (*Scalopus aquaticus*). *Journal of Morphology* 274: 1277–1287. https://doi.org/10.1002/jmor.20178

Rupert, J.E., Rose, J.A., Organ, J.M. & Butcher, M.T. (2015) Forelimb muscle architecture and composition in the groundhog (*Marmota monax*). *Journal of Experimental Biology*. 218: 194-205. https://doi.org/10.1242/jeb.107128

Sacks, R.D. & Roy, R.R. (1982) Architecture of the hindlimb muscles of cats: functional significance. *Journal of Morphology* 173: 185–195 https://doi.org/10.1002/jmor.1051730206

Sahd, L., Bennett, N.C. & Kotzé, S. H. (2020). Hind foot drumming: Morpho-functional analysis of the hind limb osteology in three species of African mol-rats (Bathyergidae). *Journal of Morphology* 281 (4-5): 438-449

Sahd, L., Bennett, N.C. & Kotzé, S.H. (2019) Hind foot drumming: morphological adaptations of the muscles and bones of the hind limb in three African mole-rat species. *Journal of Anatomy* 235: 811-824

Sahd, L., Bennett, N.C. & Kotzé, S.H. (2021). Hind foot drumming: Muscle architecture of the hind limb in three Bathyergidae species. *Journal of Mammalian Evolution* 28: 511-525. https://doi.org/10.1007/s10914-020-09527-4

Sahd, L., Bennett, N.C.& Kotzé, S.H. (2022a) Hind foot drumming: Volumetric micro-computed tomography investigation of the hind limb musculature of three African mole-rat species (Bathyergidae). *Journal of Anatomy*. 240 (1): 23-33. https://doi.org/10.1111/joa.13534

Sahd, L., Doubell, N. S. Bennett, N.C. & Kotzé, S. H. (2022b). Hind foot drumming: Myosin heavy chain muscle fibre distribution in the hind limb muscles of three African mole-rat species (Bathyergidae). *The Anatomical Record* 305: 170-183.

Savolainen, J. & Vornanen, M. (1995) Fiber types and myosin heavy chain composition in muscles of common shrew (*Sorex araneus*). *Journal of Experimental Zoology*, *271*(1): .27-35. https://doi.org/10.1007/BF00424812

Schiaffino, S. & Reggiani, C. (2011) Fiber types in mammalian skeletal muscles Physiological reviews. 91(4):1447-531. https://doi.org/10.1152/physrev.00031.2010

Schneider CA, Rasband WS, Eliceiri KW (2012) NIH Image to ImageJ: 25 years of image analysis. *Nature Methods* 9: 671–675. https://doi.org/10.1038/nmeth.2089

Serrano, A.L., Perez, M., Lucia, A.C., Chicharro, J.L., Quiroz-Rothe, E. & Rivero, J.L. (2001) Immunolabelling, histochemistry and in situ hybridisation in human skeletal muscle fibres to detect myosin heavy chain expression at the protein and mRNA level. *The Journal of Anatomy*. 199: 329-37. https://doi.org/10.1017/S0021878201008056

Sharir, A., Milgram, J. & Shahar, R. (2006) Structural and functional anatomy of the neck musculature of the dog (*Canis familiaris*). *Journal of Anatomy* 208: 331-351. https://doi.org/10.1111/j.1469-7580.2006.00533.x

Skinner, J.D. & Smithers, R.H.N. (1990) The mammals of the southern African subregion. Cape and Transvaal Printers, Pretoria, South Africa.

Suzuki, M. (1990) Fractal decomposition of exponential operators with applications to many-body theories and Monte Carlo simulations. *Physics Letters A*, 146: 319-323. https://doi.org/10.1016/0375-9601(90)90962-N

Talbot, J. & Maves, L. (2016) Skeletal muscle fibre type: using insights from muscle developmental biology to dissect targets for susceptibility and resistance to muscle disease. *Wiley Interdisciplinary Reviews-Developmental Biology* 5: 518-534. https://doi.org/10.1002/wdev.230

Tavares, W.C. & Seuánez, H.N. (2018) Changes in selection intensity on the mitogenome of subterranean and fossorial rodents respective to aboveground species. *Mammalian Genome*. 29:353-63. https://doi.org/10.1007/s00335-018-9748-5

Thomas, D.R., Chadwell, B.A., Walker, G.R., Budde, J.E., VandeBerg, J.L. & Butcher, M.T. (2016) Ontogeny of myosin isoform expression and prehensile function in the tail of the gray short-tailed opossum (*Monodelphis domestica*). *Journal of Applied Physiology* 123:513-525. https://doi.org/10.1152/japplphysiol.00651.2016

Van Wassenbergh, S., Heindryckx, S. & Adriaens, D. (2017). Kinematics of chisel-tooth digging by African mole-rats. *Journal of Experimental. Biology* 220: 4479–4485

von Mering, F. & Fischer, M.S. (1999) Fibre type regionalization of forelimb muscles in two mammalian species, *Galea musteloides* (Rodentia, Caviidae) and *Tupaia belangeri* (Scandentia, Tupaiidae) with comments on postnatal myogenesis. *Zoomorphology* 119: 117-126. https://doi.org/10.1007/s004350050086

Ward, S.R. & Lieber, R.L. (2005) Density and hydration of fresh and fixed skeletal muscle. *Journal of Biomechanics* 38: 2317– 2320. https://doi.org/10.1016/j.jbiomech.2004.10.001

Wickham, H. (2016). ggplot2: Elegant graphics for data analysis. New York: Springer-Verlag.

Williams, S.B., Payne, R.C. & Wilson, A.M. (2007) Functional specialization of the thoracic limb of the hare (*Lepus europeus*). *Journal of Anatomy* 210: 491–450. https://doi.org/10.1111/j.1469-7580.2007.00703.x

Winters, T.M., Takahashi, M., Lieber, R.L. & Ward, S.R. (2010) Whole muscle length-tension relationships are accurately modelled as scaled sarcomeres in rabbit hindlimb muscles. *Journal of Biomechanics* 44: 109–115. https://doi.org/10.1016/j.jbiomech.2010.08.033

Woods, C. A. (1975). The hyoid, laryngeal and pharyngeal regions of bathyergid and other selected rodents. *Journal of Morphology*, 147: 229–250. https://doi.org/10.1002/jmor.1051470208

Yan, Z., Okutsu, M., Akhtar, Y.N. & Lira, V.A. (2011) Regulation of exercise induced fiber type transformation, mitochondrial biogenesis, and angiogenesis in skeletal muscle. *Journal of Applied Physiology*. 110: 264-274. https://doi.org/10.1152/japplphysiol.00993.2010